NACA RM A51A16

RESEARCH MEMORANDUM

LOW-SPEED INVESTIGATION OF A 0.16-SCALE MODEL OF THE X-3 AIRPLANE - LATERAL AND DIRECTIONAL CHARACTERISTICS

By Noel K. Delany and Nora-Lee F. Hayter

Ames Aeronautical Laboratory
Moffett Field, Calif.

NATIONAL ADVISORY COMMITTEE
FOR AERONAUTICS

WASHINGTON
March 16, 1951

NATIONAL ADVISORY COMMITTEE FOR AERONAUTICS

RESEARCH MEMORANDUM

LOW-SPEED INVESTIGATION OF A 0.16-SCALE MODEL OF THE X-3 AIRPLANE - LATERAL AND DIRECTIONAL CHARACTERISTICS

By Noel K. Delany and Nora-Lee F. Hayter

SUMMARY

A wind-tunnel investigation has been made of the low-speed, static, lateral and directional characteristics of a model of an early design of the X-3 airplane with the wing flaps neutral and deflected. Measurements were also made of the fluctuations in rolling moment with time.

The model utilized a wing having an aspect ratio of 3.01, a 4.5-percent-thick hexagonal section, and a taper ratio of 0.4. The wing was equipped with plain leading-edge flaps and split trailing-edge flaps.

For all conditions investigated the data indicate that an airplane corresponding to the model tested will possess static lateral and directional stability and that the ailerons will produce satisfactory maximum values of $pb/2V$. Full rudder deflection will be sufficient to balance the airplane to 8° of sideslip. As indicated by the measured fluctuating rolling moments, the airplane may possess undesirable rolling-moment characteristics near and after the stall with the flaps fully deflected.

INTRODUCTION

The X-3 airplane, designed as a supersonic research airplane incorporating such features as a thin low-aspect-ratio wing and a large fuselage, might be expected to present stability problems in low-speed flight. The low-speed longitudinal characteristics as measured with a 0.16-scale model are presented in reference 1. References 2, 3, and 4 present the aerodynamic characteristics of the same model of the X-3 airplane at high subsonic speeds as measured in the Ames 16-foot high-speed wind tunnel. Since the construction and testing of the model referred to herein and in references 1, 2, 3, and 4, the design of the fuselage, wing, and empennage have been modified.

In conjunction with the determination of the low-speed longitudinal characteristics (reference 1) the lateral and directional stability and control characteristics of the model were determined and are presented in the present report. The data indicate the effects of the component parts of the model on the static lateral and directional stability and show the control effectiveness of the ailerons and rudder. During the investigation, large erratic rolling moments were encountered near the stall. These rolling moments were investigated in some detail and the results are presented herein.

The tests were conducted in the Ames 7- by 10-foot wind tunnel.

COEFFICIENTS AND SYMBOLS

The center of gravity assumed for the reduction of the data to coefficient form was on the fuselage reference line and 0.15 of the wing mean aerodynamic chord behind the leading edge of the wing mean aerodynamic chord. Rolling-moment coefficients were computed about an axis coincident with the fuselage reference line. Yawing moments were computed about an axis in the plane of symmetry, normal to the free-stream direction and passing through the moment center. Figure 1 shows the sign conventions used for forces, moments, control-surface deflections, angle of pitch, and angle of yaw.

The following coefficients and symbols are used in this report:

C_L lift coefficient $\left(\frac{\text{lift}}{qS}\right)$

c_l section-lift coefficient $\left(\frac{\text{section lift}}{qc}\right)$

C_l rolling-moment coefficient $\left(\frac{\text{rolling moment}}{qSb}\right)$

C_n yawing-moment coefficient $\left(\frac{\text{yawing moment}}{qSb}\right)$

$C_{l_{\delta_a}}$ rate of change of rolling-moment coefficient with aileron angle, per degree

$C_{l_{\delta_r}}$ rate of change of rolling-moment coefficient with rudder angle, per degree

$C_{n_{\delta_r}}$ rate of change of yawing-moment coefficient with rudder angle, per degree

C_{l_ψ} rate of change of rolling-moment coefficient with angle of yaw, measured between 0° and 5° angle of yaw unless otherwise specified, per degree

C_{l_p} rate of change of rolling-moment coefficient with $\frac{pb}{2V}$, per radian

C_{n_ψ} rate of change of yawing-moment coefficient with angle of yaw, measured between 0° and 5° angle of yaw unless otherwise specified, per degree

$\frac{pb}{2V}$ helix angle generated by the wing tip in roll, radians

q free-stream dynamic pressure $\left(\frac{1}{2}\rho V^2\right)$, pounds per square foot

ρ mass density of the air in the free stream, slugs per cubic foot

V free-stream velocity, feet per second

p angular velocity in roll, radians per second unless otherwise specified

S wing area, leading and trailing edges projected to plane of symmetry, square feet

b span of the wing, feet

$\bar{c}$ mean aerodynamic chord of the wing $\left(\frac{\int_0^{0.5b} c^2 dy}{\int_0^{0.5b} c\, dy}\right)$, feet

c local chord of the wing, feet

f frequency, cycles per second

Δt increment of time, seconds

y lateral distance measured from plane of symmetry, feet

α angle of attack of the fuselage reference line, degrees

$\Delta\alpha$ increment of angle of attack, degrees

δ_{LF} deflection of the leading-edge flap, positive downward, degrees

δ_{TF} deflection of split trailing-edge flap, positive downward, degrees

δ_a aileron deflection, degrees

δ_r rudder deflection, degrees

ψ angle of yaw, degrees

MODEL AND APPARATUS

The model used for this investigation is the one described in reference 1. (However, since the construction and testing of the model, the airplane design has been considerably modified.) A diagrammatic sketch of the model is shown in figure 2. The model is shown mounted in the wind tunnel in figure 3 and pertinent geometric characteristics of the model are presented in table I. The complete model consisted of the wing, fuselage, and tail as defined in reference 1. The fuselage included the tail boom unless otherwise noted.

The left wing of the model was equipped with an aileron of 25-percent chord which could be deflected 5°, 10°, or 15° in either direction. The span of the aileron was 30 percent of the wing semispan and the aileron extended from the wing tip to the trailing-edge flap.

The wing of the model was equipped with flush orifices for measuring the pressure distribution. These orifices were arranged in chordwise rows at the spanwise locations indicated in figure 4.

Because of the model structure, it was not possible to test the wing of the model alone. Therefore, a wing identical in plan form and section to that of the model was constructed for use in tests of an isolated wing. The isolated wing was not, however, equipped with an aileron or with orifices for measuring the pressure distribution.

To permit determination of the effects of the component parts of the fuselage on the stability, the tail boom was removable and the model was constructed so that the aft 9.3 percent of the body, based on the body length, could be removed. The body-boom assembly is indicated in figure 5.

The rudder, which had a span equal to 74.5 percent of the span of the vertical tail and an average chord equal to 38.1 percent of the average chord of the vertical tail could be deflected 20° either to the right or to the left. The rudder hinge line was normal to the fuselage reference line.

The arrangement of the main landing gear and the main landing-gear doors (denoted in reference 1 as main-gear door configuration 1) is shown in figure 6(a). The nose landing gear and nose landing-gear door are shown in figure 6(b). The canopy, air scoops, and jettisonable-nose fins are shown in figures 7(a), 7(b), and 7(c). The air scoops (fig. 7(b)) were made with recessed faces and without ducts; there was no internal flow. Due to the manner in which the model was constructed, it was impossible to test the complete model with the canopy (fig. 7(a)) and the air scoops (fig. 7(b)) installed simultaneously. For pilot escape at supersonic speeds the nose of the airplane, including the pilot's enclosure, was originally designed to be jettisonable. Stabilizing fins (fig. 7(c)) for the jettisonable-nose section were tested on the model. The arrangement tested was that designated as the normal position of the fins in reference 2.

The models (complete model and isolated wing) were mounted on single support struts as shown in figure 3. For the complete model the support strut had a round cross section and was directly below the moment center. For the isolated wing, however, the support strut had an airfoil section that yawed as the model was yawed, and was attached to the model at a point behind the moment center.

Yawing moments were measured with the wind-tunnel balance system. Rolling moments were measured by means of a resistance-type strain gage mounted within the model and a highly damped light-beam galvanometer. For the investigation of rolling-moment oscillations the strain-gage support system was made much stiffer, thereby decreasing the motions of the model, and the output from the rolling-moment strain gage was recorded as a function of time by an oscillograph.

CORRECTIONS TO DATA

The angle of attack has been corrected for the effects of tunnel-wall interference by the method of reference 5 by adding the following correction:

$$\Delta\alpha = 0.382\ C_L$$

Corrections to the angle of yaw, rolling-moment coefficients, and yawing-moment coefficients due to the tunnel-wall interference, were not applied as they were negligible.

None of the data except those obtained with the isolated wing have been corrected for the effects of the model-support strut. For the complete model, significant effects of the support on the moments presented herein would not be anticipated. For the isolated wing, however,

it was necessary to correct the yawing moments for tares of the single support strut. Previous test data indicated the rolling-moment tares were negligible.

RESULTS AND DISCUSSION

The static lateral- and directional-stability and -control characteristics indicated by the tests of the 0.16-scale model are presented in figures 8 to 21. The test Reynolds number, based on the wing mean aerodynamic chord, was approximately 2.0×10^6. Figures 22 through 28 present the data obtained during the investigation of the oscillating rolling moments. The Reynolds number for this investigation was approximately 1.4×10^6.

Lateral Stability and Control With the Flaps Neutral

The contributions of the component parts of the model to the static lateral stability with the flaps neutral are shown in figure 8(a). The fuselage without the tail boom had approximately neutral lateral stability at small angles of yaw. By the addition of the boom, the stability of the fuselage was increased to $C_{l_\psi} = 0.0005$. The variation with angle of yaw of the rolling-moment coefficient due to the tail boom was also computed by means of the method of reference 6 using the data of reference 7 and assuming the tail boom to act as a highly swept wing lying in a vertical plane. The assumed root chord of the boom was parallel to the horizontal-tail reference plane and passed through the point of intersection of the leading edge of the boom and the top of the fuselage. The tip chord of the boom was assumed in the reference plane of the horizontal tail. The computed variation of rolling-moment coefficient with angle of yaw agreed with the measured value.

The wing alone had approximately the same degree of lateral stability (fig. 8(a)) as the fuselage with the tail boom. The complete model without the tail, however, was neutrally stable due to the destabilizing wing-fuselage interference. The variations of the section-lift coefficient, evaluated from pressure-distribution data, with angle of yaw for three spanwise stations along the wing (fig. 9) indicate that the wing-fuselage interference in yaw resulted in a decrease in lift on the leading wing and an increase in lift on the trailing wing with a resultant destabilizing dihedral effect. The decrease in lift on the leading wing and the increase in lift on the trailing wing may be explained by considering the induced effects of the fuselage. As the model was yawed, the cross flow normal to the plane of symmetry increased, thereby

causing increases in the induced angles of attack due to the fuselage. Since the wing was attached to the lower half of the fuselage the leading wing experienced a decrease in angle of attack, induced by the fuselage, with increasing angle of yaw and the trailing wing experienced a converse effect.

The addition of the vertical tail increased the lateral stability of the complete model to $C_{l_\psi} = 0.0025$ (fig. 8(a)). The large contribution of the vertical tail to the lateral stability was due to the height of the center of pressure on the vertical tail above the roll axis. The addition of the horizontal tail had a negligible effect on the static lateral stability (fig. 8(a)).

The effect of angle of attack on the static lateral stability of the complete model is shown in figure 10(a). The stability increased with increasing angle of attack. For angles of attack from 0° to 10° the increase was approximately linear with angle of attack. Above an angle of attack of 10° the rate of increase was more rapid.

The variation of aileron effectiveness with angle of attack for the complete model without the tail is presented in figure 11. Between angles of attack of 0° and [1]12° the aileron effectiveness remained approximately constant ($C_{l_{\delta_a}} = 0.0011$ at $\alpha = 0°$ to $C_{l_{\delta_a}} = 0.0009$ at $\alpha = 12°$). After the stall ($\alpha = 12°$) the value of $C_{l_{\delta_a}}$ decreased to approximately 0.0006 with the model at an angle of attack of 14°. The data also indicate that some aileron effectiveness was maintained up to the maximum test angle of attack ($\alpha = 23°$).

From these test results, values of maximum $pb/2V$ with the rudder locked were estimated for 250 and 650 miles per hour using values of C_{l_p} of −0.20 and −0.27, respectively. The maximum values of $pb/2V$ were estimated to be 0.16 at both 250 miles per hour and 650 miles per hour. This value of $pb/2V$ exceeds the minimum requirements of reference 8 which specifies that the minimum value of $pb/2V$ shall be 0.090. The rolling velocities corresponding to these estimated values of $pb/2V$ are 310° and 795° per second, respectively. Due to the small span of the wing, the parameter $pb/2V$ may not be a good criterion of the rolling effectiveness of the ailerons as the estimated rolling velocities are higher than those normally encountered with conventional airplanes.

---

[1]With the flaps neutral the model stalled at an angle of attack of approximately 12° where stall is herein defined as the condition where the slope of the lift curve first becomes zero at a positive angle of attack.

The yawing moments due to aileron deflection, below the stall, were not adverse but are not presented since they were too small to be determined accurately by the measuring equipment.

Lateral Stability and Control With the Flaps Fully Deflected

The contributions of the component parts of the model to the static lateral stability with the leading- and trailing-edge flaps deflected 30° and 50°, respectively, are shown in figure 8(b). The wing with the flaps deflected had approximately the same lateral stability as with the flaps neutral. The complete model without the tail, with flaps deflected, was slightly unstable (C_{l_ψ} = −0.00006) for angles of yaw between ±5°. With the addition of the landing gear and landing-gear doors, the complete model without the tail became neutrally stable, indicating that the main landing gear and main landing-gear doors decreased the destabilizing wing-fuselage interference. (From data not presented, it was found that the nose landing gear and nose landing-gear door did not influence the lateral stability.) The contribution of the tail to the lateral stability of the model with the flaps deflected (fig. 8(b)) was approximately the same as with the flaps neutral (fig. 8(a)). The effect of angle of attack on the static lateral stability of the complete model with the flaps deflected, shown in figure 10(b), was approximately the same as with the flaps neutral. The lateral stability increased from approximately C_{l_ψ} = 0.0029 for an angle of attack of 0° to approximately C_{l_ψ} = 0.0053 for an angle of attack of 15°.

In figure 11(b) is shown the variation of aileron effectiveness with angle of attack for the complete model without the tail, with the leading- and trailing-edge flaps fully deflected. Between 0° and 12° angle of attack of the model the aileron effectiveness increased ($C_{l_{\delta_a}}$ = 0.0009 at 0° to $C_{l_{\delta_a}}$ = 0.0013 at 12° angle of attack). Beyond 12° the aileron effectiveness decreased to approximately 0.0009 at 18° angle of attack. Above 18° angle of attack of the model (the approximate stalling angle with the flaps fully deflected) the measured rolling moments and aileron effectiveness became very erratic. In the section entitled "Oscillating Rolling Moments," the rolling moments near and above the stall will be discussed in more detail.

By use of the aileron-effectiveness data of figure 11(b) and a value of C_{l_p} of −0.237, the maximum value of $pb/2V$ with the rudder locked for an airplane flight speed of 200 miles per hour at sea level is estimated to be 0.136 for full aileron deflection. The value of the rolling velocity p corresponding to the above value of $pb/2V$ is 209° per

second. This estimated value of $pb/2V$ satisfies the requirements of reference 8.

As was the case with the flaps neutral, the yawing moments due to aileron deflection have not been presented since the measured values, below the stall, were not adverse and were too small to be determined accurately. After the stall, however, there were indications in the data that the yawing moments may become quite erratic and of larger magnitude. This was attributed to the same causes as were the oscillating rolling moments which will be discussed later.

Lateral Stability With Miscellaneous Additions to the Complete Model

The effects on the lateral stability of the addition of the canopy, the air scoops, or the jettisonable-nose fins to the complete model are presented in figures 12 to 14. The effects of these additions to the model were small with the flaps neutral or deflected. The effect of the air scoops may not have been representative as there was no air flow into the scoops. The jettisonable-nose fins did not affect the lateral stability. As noted in reference 1, however, the nose fins were abandoned because of their adverse effect on the longitudinal stability.

Directional Stability and Control With the Flaps Neutral

The contributions of the component parts of the model to the static directional stability with flaps neutral are presented in figure 15(a). The fuselage, without the tail boom and the aft 9.3 percent of the body, was unstable ($C_{n_\psi} = 0.0026$). The addition of the aft 9.3 percent of the fuselage decreased the directional instability of the fuselage when yawed more than 8°; the further addition of the tail boom caused a large reduction in the instability of the fuselage, contributing a yawing moment equivalent to approximately 20 percent of that produced by the vertical tail. The contribution of the tail boom was computed considering the boom as a highly swept wing as described previously. The computed value ($C_{n_\psi} = -0.0021$) was in good agreement with the measured value ($C_{n_\psi} = -0.0020$). The wing was neutrally stable. The directional instability of the complete model without the tail was approximately the same as that of the fuselage, indicating little interference between the wing and fuselage in this respect. The stabilizing effect of the vertical tail on the complete model is larger than normal. However this size tail may be required for satisfactory operation of the airplane at design supersonic speeds. The addition of the horizontal tail to the model had little

effect on the directional stability (fig. 15(a)). For small angles of yaw, ±5°, the directional stability remained essentially constant throughout the angle-of-attack range of 0° to 15° (fig. 16(a)).

The effect of rudder deflection on the directional characteristics of the complete model with flaps neutral is shown in figure 17(a). Due to the high directional stability ($C_{n_\psi} = -0.0089$) it was possible to balance the model only to 8° of yaw. This angle of yaw does not satisfy the requirement of reference 8 which specifies that full rudder deflection shall produce at least 10° of steady sideslip. However, the applicability of the requirement of reference 8 may be subject to question for an airplane of this type.

Negative deflection of the rudder produced a large negative change in rolling moments (fig. 18(a)) such that $C_{l_{\delta_r}}$ was approximately equal and opposite to the effectiveness of the ailerons ($C_{l_{\delta_r}} = 0.001$ from figure 18(a)). Superimposed on the curves of rolling-moment coefficient as a function of angle of yaw for constant rudder deflection is a curve of zero yawing-moment coefficient. These data indicate that, with the ailerons held neutral, if the rudder is suddenly deflected to the right the airplane will start to roll to the left and yaw to the right, then roll to the right as the airplane approaches the angle of yaw at which it will balance for the given rudder deflection. Even without an analysis of the dynamic motions of the airplane it may be inferred that coordinated turns might be difficult to achieve.

Directional Stability and Control With the Flaps Fully Deflected

In figure 15(b) are shown the contributions of the various parts of the model to the directional stability with leading- and trailing-edge flaps deflected. The wing and the complete model without the tail had approximately the same small degree of stability ($C_{n_\psi} = -0.0003$) for angles of yaw of ±5°. The instability which resulted from the addition of the landing gear and landing-gear doors to the model ($C_{n_\psi} = 0.0012$) was attributed mainly to the nose wheel and door which were 0.85 of the wing span ahead of the moment center. The directional stability of the complete model with the flaps deflected was approximately the same as that of the complete model with flaps neutral ($C_{n_\psi} = -0.0089$) and, for small angles of yaw, was approximately constant throughout the angle-of-attack range of 0° to 15° (fig. 16).

There was no significant change in rudder effectiveness due to the deflection of the leading- and trailing-edge flaps (fig. 17). The

variation of rudder effectiveness with angle of attack, although not presented, was approximately constant to the stall beyond which point the data were probably unreliable as is explained in the section entitled "Oscillating Rolling Moments." The variation of rolling-moment coefficient with angle of yaw with the yawing moments balanced by rudder deflection (fig. 18(b)) indicates that the airplane with the flaps fully deflected will react to deflection of the rudder in a manner similar to that previously discussed for the case of the flaps neutral.

Directional Stability With Miscellaneous Additions to the Complete Model

The effects on the directional stability of the addition of the canopy, the air scoops, or the jettisonable-nose fins to the complete model both with flaps neutral and deflected are presented in figures 19 to 21. There was no change in the directional stability of the model for angles of yaw of -5° to $\pm 5^\circ$ with flaps neutral or deflected due to the addition of the canopy or the air scoops. The addition of the nose fins decreased the directional stability of the model with flaps neutral or deflected (fig. 21). This decrease in stability was attributed to the forces acting on the nose fins ahead of the moment center. In reference 1 a similar decrease in longitudinal stability was attributed to the lift forces acting on the fins.

Oscillating Rolling Moments

As previously mentioned, the measured rolling moments near or above the wing stall, for the model with the flaps fully deflected ($\delta_{LF} = 30^\circ$, $\delta_{TF} = 50^\circ$) were quite erratic as indicated by the strain-gage equipment for measuring rolling moments. Recourse was therefore made to the use of an oscillograph which recorded the output from the rolling-moment strain gage as a function of time. An attempt was made to determine the electronic and mechanical characteristics of the experimental setup and thus the relationship between the indicated and the actual oscillating rolling moment. Figure 22 shows the experimentally determined calibration factor (factor by which the indicated rolling moment should be multiplied to ascertain the actual rolling moment) as a function of the frequency of oscillation. Also shown in figure 22 are the contributions of the mechanical portion of the system (stiffened strain-gage system in combination with the model) and of the electronic equipment (oscillograph, filter, and amplifier) to the calibration factor. From these data it appears that the natural frequency of the model in roll on the support system was 23.5 cycles per second. Also, for frequencies from 0 to 9.5 cycles per second the indicated rolling-moment coefficients appear to be

within 10 percent of the actual coefficients. The calibration factor has not been applied to the data; however, it has been included to permit a better understanding of the measurements of the oscillating rolling moments. Figures 23 to 28 are reproductions of typical portions of the oscillograph records for various model configurations but do not necessarily present the maximum rolling-moment coefficients observed for a given model configuration.

Fuselage alone.- Figures 23 and 24 show the variation of rolling-moment coefficient with time in seconds for the fuselage (body and boom, see fig. 5) and for the fuselage with the tail on, for angles of attack of 8° to 26°. For the fuselage alone at an angle of attack of 8°, the oscillating rolling moment was negligible; at 16° angle of attack a small-amplitude oscillation became apparent with a frequency varying between 40 cycles and 60 cycles per second. As the angle of attack was increased to 26°, a larger oscillation of the rolling-moment coefficient developed that had an amplitude of approximately ± 0.02 and a frequency of approximately 3 to 6 cycles per second. With the vertical tail on the fuselage (fig. 24), the development of the oscillating rolling moments followed the same pattern. However, the amplitudes became increasingly larger, reaching values as high as $\Delta C_l = \pm 0.07$. It is believed that the low-frequency oscillating rolling moments were caused by intermittent discharge of vortices from the sides of the fuselage, possibly in a manner similar to that for bodies of revolution noted in reference 9. With the vertical tail on the fuselage, the vortices impinged on the tail, increasing the amplitude of the rolling moments. Visual studies at low wind-tunnel speeds were made using two filaments of smoke. These observations indicated two vortices to be forming on the forward portion of the fuselage and discharging alternately from the sides of the fuselage at approximately the point of maximum fuselage breadth. The vortex that was not being discharged appeared to decay and intermingle with the turbulent fuselage wake.

Complete model - flaps neutral.- The data for the complete model, tail off and tail on, are presented in figures 25 and 26 for angles of attack of 8.3° to 20.6°. Above 20.6° angle of attack the oscillations did not increase in amplitude, nor did the amplitude of the rolling-moment oscillation for the model become as large as for the fuselage alone or for the fuselage with the tail on. It is possible that the reason the oscillations were smaller was that the large wake from the stalled wing caused a rapid decay or breaking up of the vortices being discharged by the fuselage.

Complete model - flaps fully deflected.- With the wing leading- and trailing-edge flaps deflected 30° and 50°, respectively (figs. 27 and 28), large rolling-moment oscillations ($\Delta C_l = \pm 0.05$) were indicated for angles of attack of 19.4° and 20.4°. For larger angles of attack up to 26° the

rolling-moment oscillations were abated to some extent. The vertical tail did not seem to influence the magnitude of the rolling moments, nor did the rolling moments tend to be cyclic as was the case for the fuselage and tail. It is believed that the vortices shed from the wing flaps interacted with the fuselage vortices so that irregular and intermittent rolling-moment oscillations occurred. This hypothesis was partially verified by smoke studies that showed large vortices being steadily discharged from the outer ends of the trailing-edge flaps even after the wing stalled. These vortices from the flaps appeared to be intermittently drawn into the vortices from the fuselage.

Although the measurements of the oscillating rolling moments were made at a comparatively low Reynolds number (1.4×10^6, based on the wing mean aerodynamic chord), it appears possible that increases of Reynolds number will not greatly influence the results. This is believed possible because of the shape of the fuselage cross section and of the three-dimensional development of the vortices which may cause the discharge to persist to indefinitely large Reynolds numbers.

It should be pointed out also that the forces acting on the fuselage, boom, and vertical tail that caused the oscillating rolling moments would also cause oscillating yawing moments. The instrumentation was not sufficiently extensive, however, to measure the variation of the yawing moments with time.

CONCLUSIONS

The following conclusions can be drawn from the low-speed tests made to ascertain the lateral and directional characteristics of a 0.16-scale model of an early design of the X-3 airplane conducted in the Ames 7- by 10-foot wind tunnel:

1. An airplane corresponding to the complete model would possess static lateral and directional stability for all conditions investigated.

2. The ailerons would produce satisfactory maximum values of $pb/2V$. However, the actual rolling velocities would be higher than those normally encountered.

3. Full rudder deflection would be sufficient to balance the airplane to only 8° of sideslip, due to the high degree of directional stability.

4. Deflection of the rudder produced large rolling moments that were approximately equal and opposite to the rolling moments produced by an equal angular deflection of the ailerons.

5. Near and after the stall with the flaps deflected, an airplane corresponding to the model might possess undesirable rolling-moment characteristics, due to fluctuating rolling moments.

Ames Aeronautical Laboratory,
National Advisory Committee for Aeronautics,
Moffett Field, Calif.

REFERENCES

1. Delany, Noel K., and Hayter, Nora-Lee: Low-Speed Investigation of a 0.16-Scale Model of the X-3 Airplane – Longitudinal Characteristics. NACA RM A50G06, 1950.

2. Hamilton, William T., and Cleary, Joseph W.: Wind-Tunnel Tests of a 0.16-Scale Model of the X-3 Airplane at High Subsonic Speeds. – Stability and Control Characteristics. NACA RM A50A03, 1950.

3. Cleary, Joseph W., and Mellenthin, Jack A.: Wind-Tunnel Tests of a 0.16-Scale Model of the X-3 Airplane at High Subsonic Speeds. – Additional Stability and Control Characteristics and the Aerodynamic effects of External Stores and Ram Jets. NACA RM A50C30, 1950.

4. Cleary, Joseph W., and Mellenthin, Jack A.: Wind-Tunnel Tests of a 0.16-Scale Model of the X-3 Airplane at High Subsonic Speeds. – Wing and Fuselage Pressure Distribution. NACA RM A50D07, 1950.

5. Swanson, Robert S., and Schuldenfrei, Marvin J.: Jet-Boundary Corrections to the Downwash Behind Powered Models in Rectangular Wind Tunnels with Numerical Values for 7- by 10-Foot Closed Wind Tunnels. NACA ARR, 1942.

6. Bauer, C.: Dynamic Lateral Stability of the MX-656 Airplane – 499D. Douglas Aircraft Co., Rep. SM 13429, Dec. 23, 1948.

7. DeYoung, John: Theoretical Additional Span Loading Characteristics of Wings With Arbitrary Sweep, Aspect Ratio, and Taper Ratio. NACA TN 1491, 1947.

8. Anon: Specification for Flying Qualities of Piloted Airplanes. Spec. No. 1815-B, U.S. Air Force, June 1, 1948.

9. Allen, Julian H., and Perkins, Edward W.: Characteristics of Flow Over Inclined Bodies of Revolution. NACA RM A50L07, 1951.

TABLE I.- GEOMETRIC CHARACTERISTICS OF THE MODEL

Wing	
Area, square feet	4.091
Aspect ratio	3.01
Taper ratio	0.4
Span, feet	3.507
Mean aerodynamic chord, feet	1.238
Root chord, feet	1.667
Tip chord, feet	0.667
Thickness, percent	4.5
Dihedral, degrees	0
Incidence, degrees	0
Sweep of 75-percent-chord line, degrees	0
Distance of wing chord plane below fuselage reference plane, feet	0.078
Wing movable surfaces	
Leading-edge flaps	
Type	plain
Wing station at inner end, feet	0.420
Wing station at outer end, feet	1.753
Chord, feet	0.167
Maximum deflection, degrees	40
Trailing-edge flaps	
Type	split
Wing station at inner end, feet	0.407
Wing station at outer end, feet	1.226
Chord, percent wing chord	25.0
Maximum deflection, degrees	60
Ailerons	
Type	plain
Wing station at inner end, feet	1.228
Wing station at outer end, feet	1.753
Chord, percent wing chord	25.0
Deflection, degrees	±15
Horizontal tail	
Area, square feet	0.794
Aspect ratio	3.01
Taper ratio	0.4
Span, feet	1.547
Root chord, feet	0.752
Tip chord, feet	0.293
Sweep of 50-percent-chord line, degrees	23
Incidence (variable), degrees	10 to -19
Mean aerodynamic chord of the exposed area, feet	0.521

TABLE I.- CONCLUDED

Horizontal tail (concluded)	
Exposed area, square feet	0.701
Hinge line, percent of M.A.C. of exposed area	25
Tail length (from 15 percent wing M.A.C. to horizontal-tail hinge line), feet	3.375
Height above fuselage reference line, feet	0.587
Vertical tail	
Area, square feet	0.678
Aspect ratio	1.32
Taper ratio	0.25
Span, feet	0.947
Root chord, feet	1.147
Tip chord, feet	0.287
Height of root chord above fuselage reference line, feet	0.688
Sweep of 90-percent-chord line, degrees	0
Mean aerodynamic chord, feet	0.803
Tail length (from 15 percent wing M.A.C. to 25 percent vertical tail M.A.C.), feet	3.411
Rudder (Hinge line normal to fuselage reference line)	
Span, feet	0.705
Tip chord, feet	0.162
Root chord, feet	0.227
Deflection, degrees	±20
Jettisonable-nose fins	
Area of each fin, square feet	0.084
Aspect ratio	0.75
Taper ratio	0.25
Span, feet	0.253
Root chord, feet	0.533
Tip chord, feet	0.133
Mean aerodynamic chord, feet	0.373
Sweep of 90-percent-chord line, degrees	0
Horizontal distance from 15-percent wing M.A.C. to 25-percent fin M.A.C., feet	1.156
Assumed wing loading, pounds per square foot	100

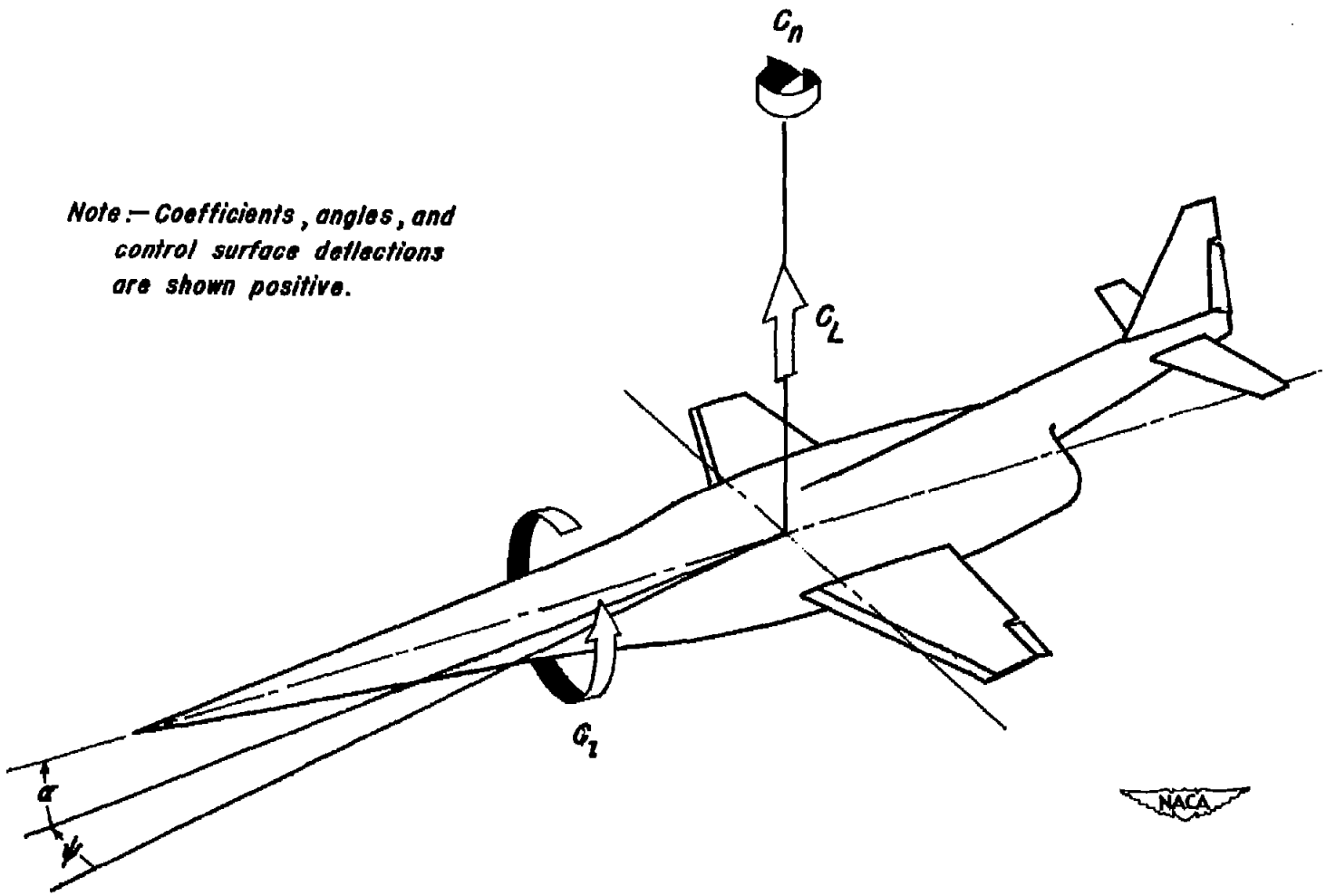

Figure 1:— Diagrammatic sketch indicating the sign conventions used.

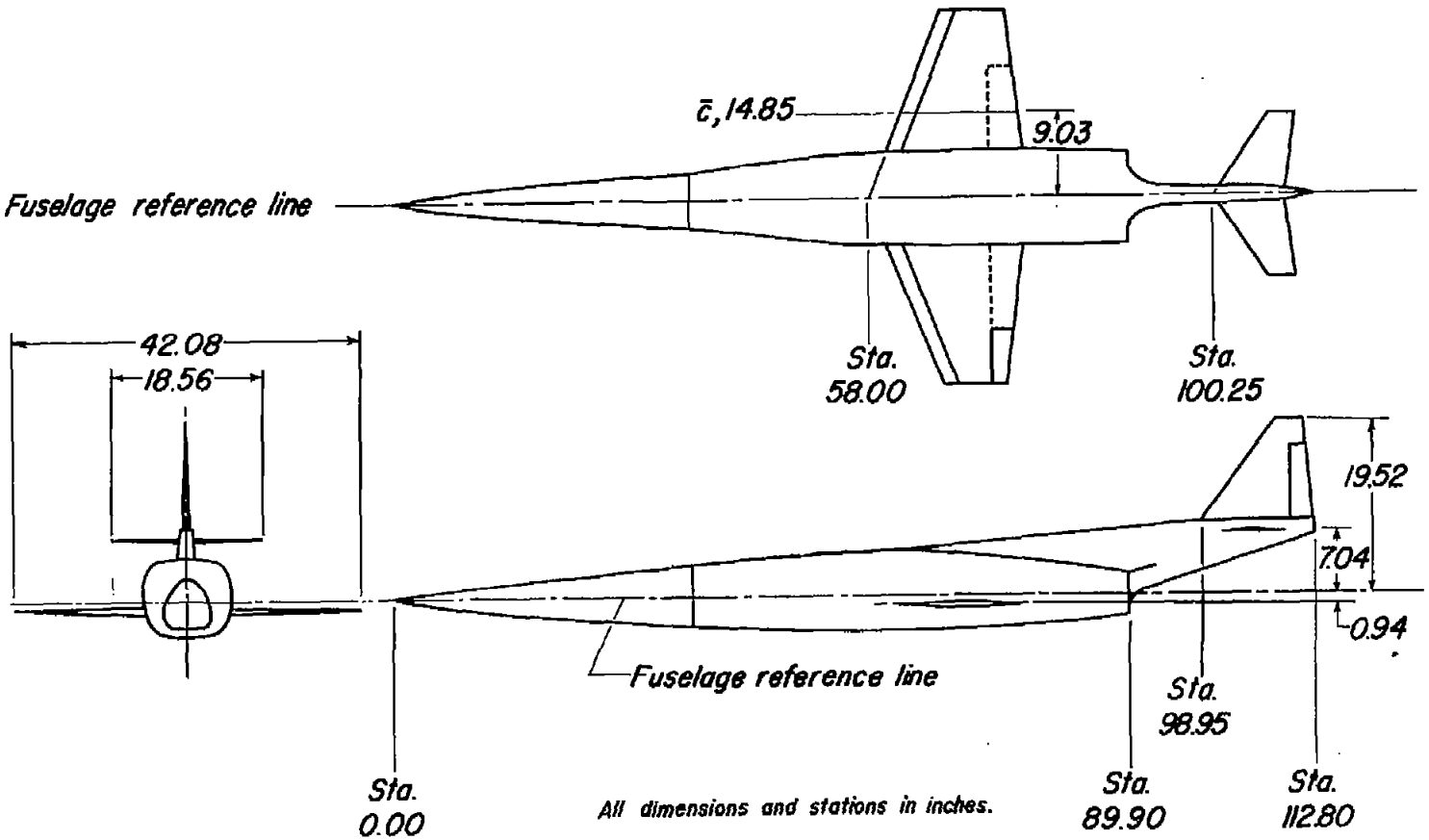

Figure 2.- Diagrammatic sketch of the model.

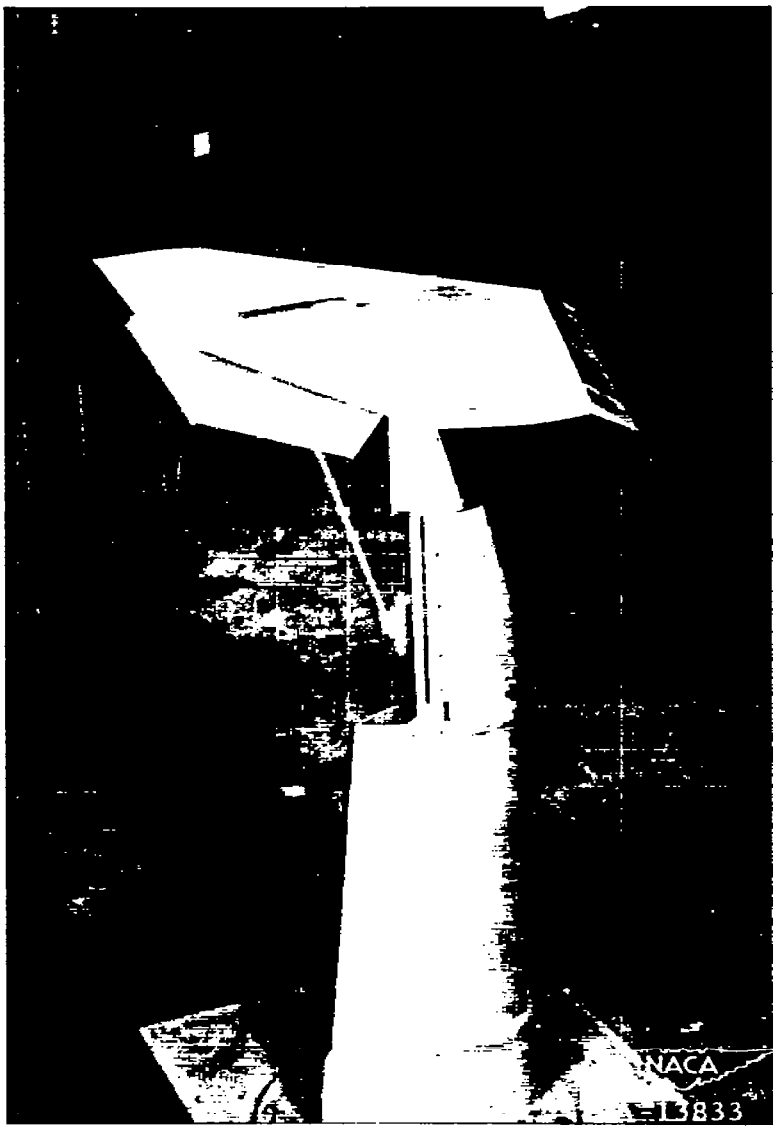

(a) Wing alone.

Figure 3.- The model in the wind tunnel.

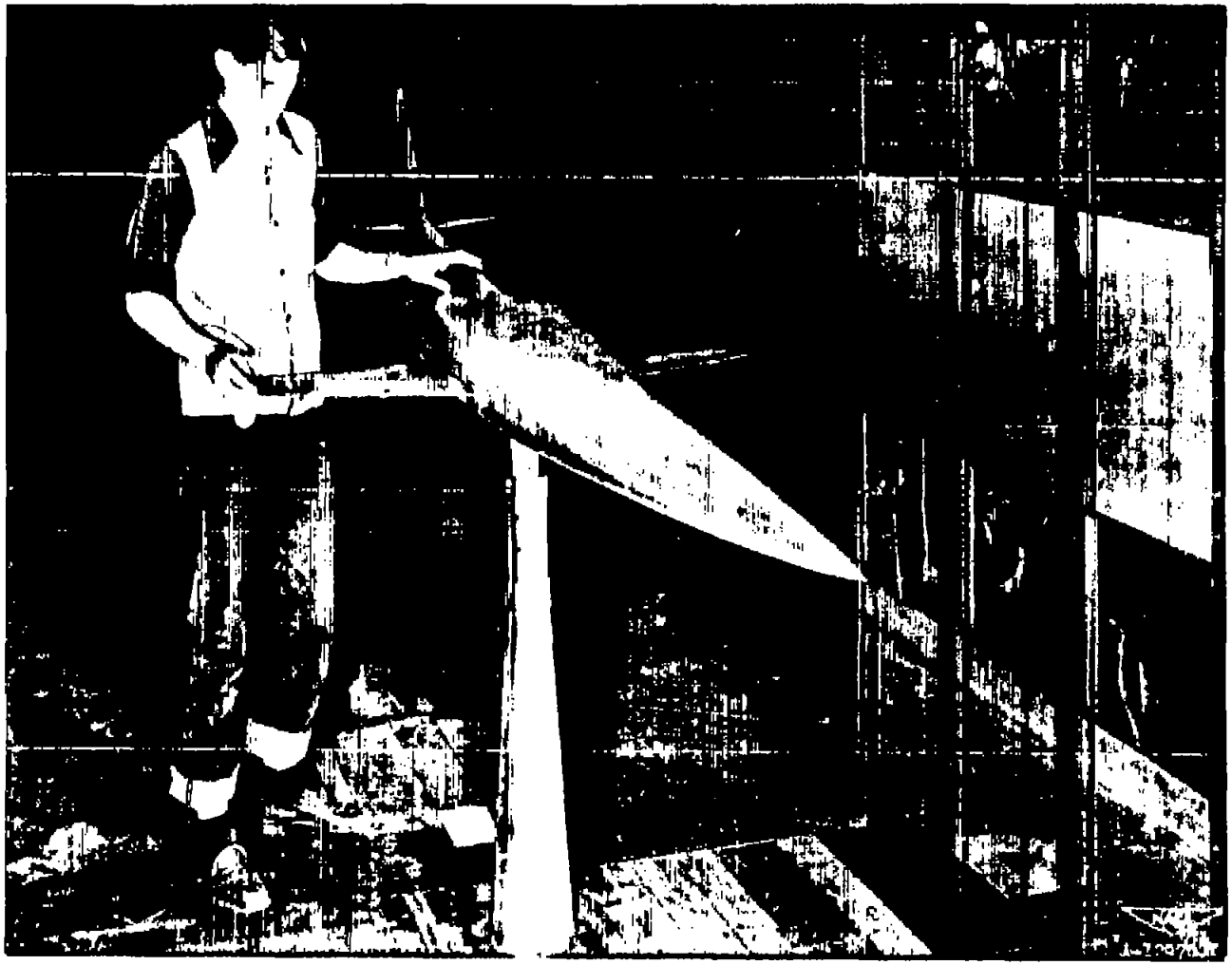

(b) Complete model, flaps neutral.

Figure 3.- Concluded.

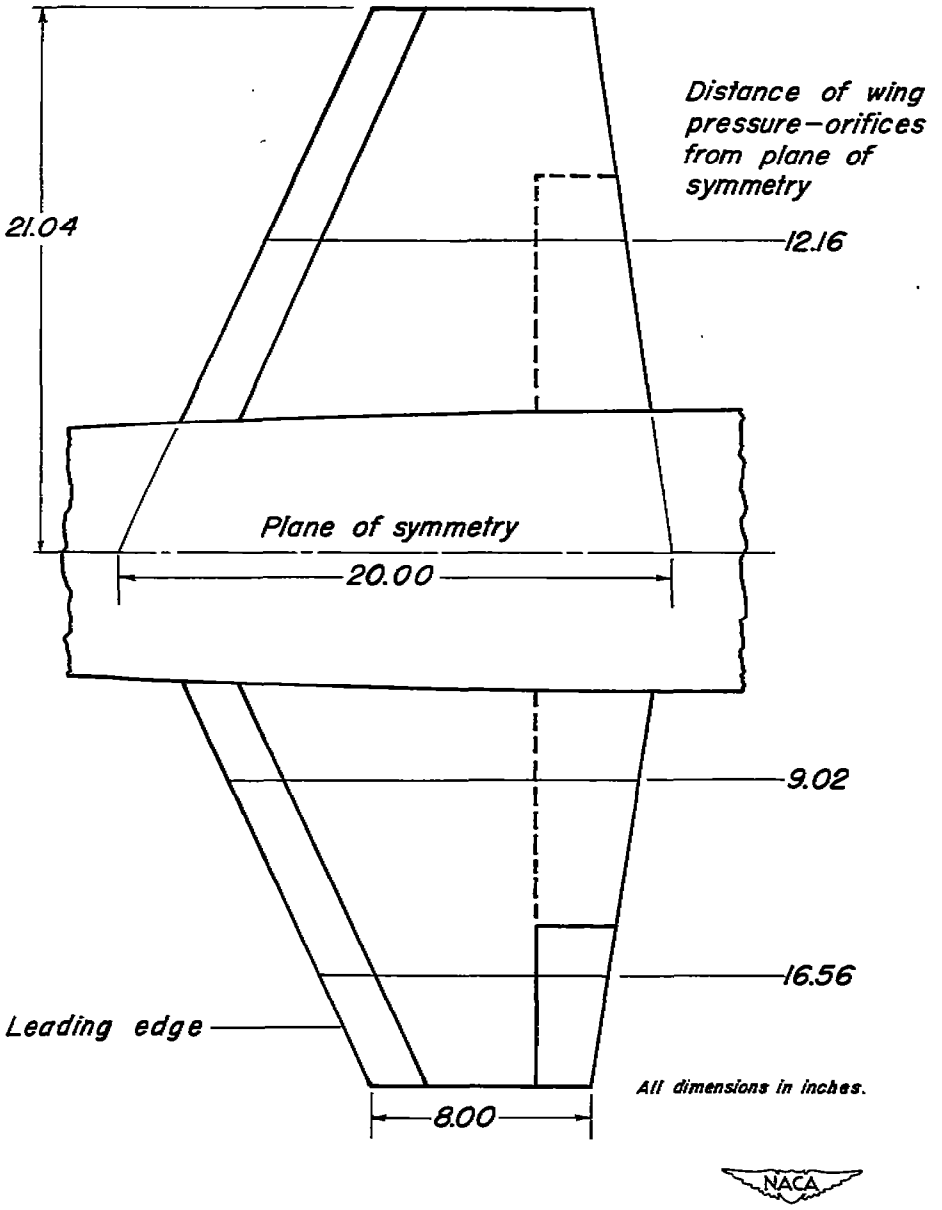

Figure 4.- Spanwise locations of the wing pressure orifices.

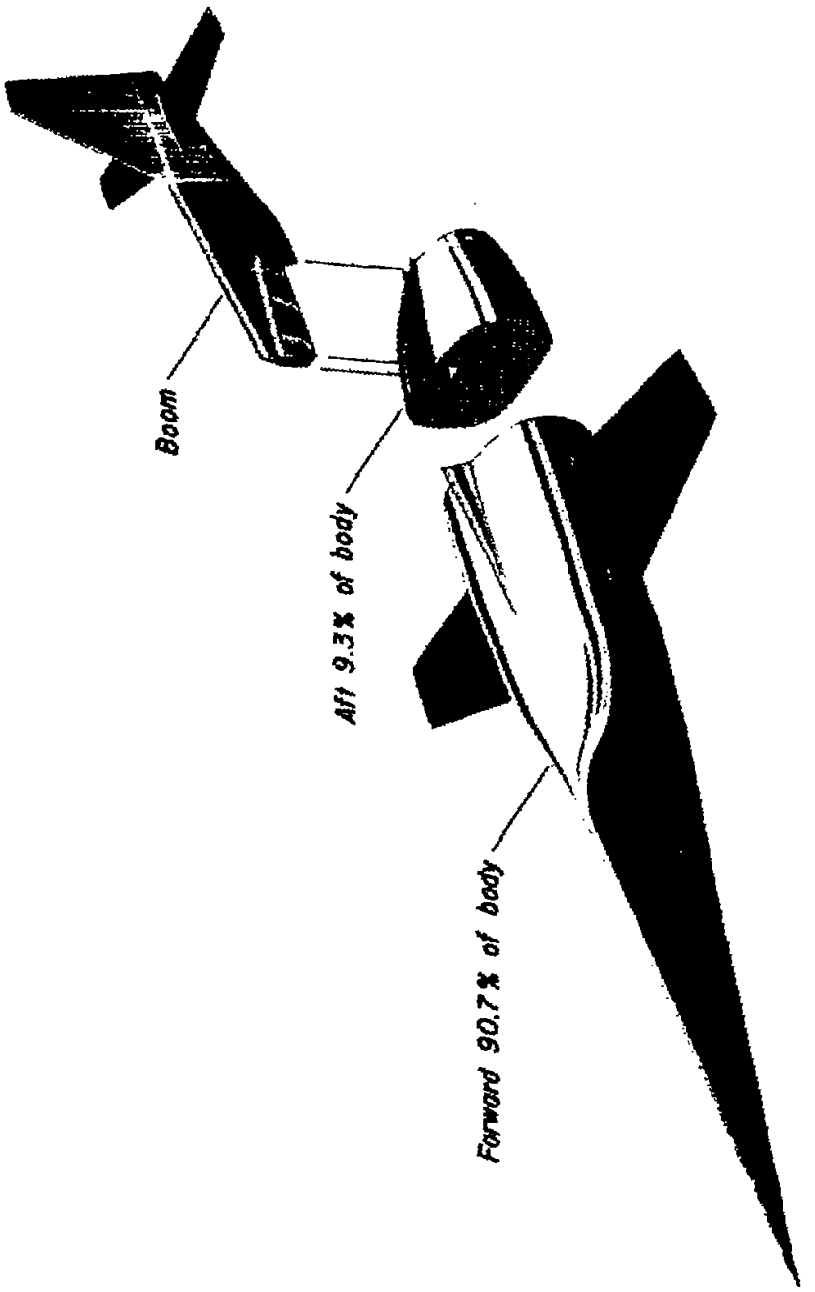

Figure 5.- Diagrammatic sketch indicating the manner in which the boom and aft 9.3 percent of the body were removed from the model.

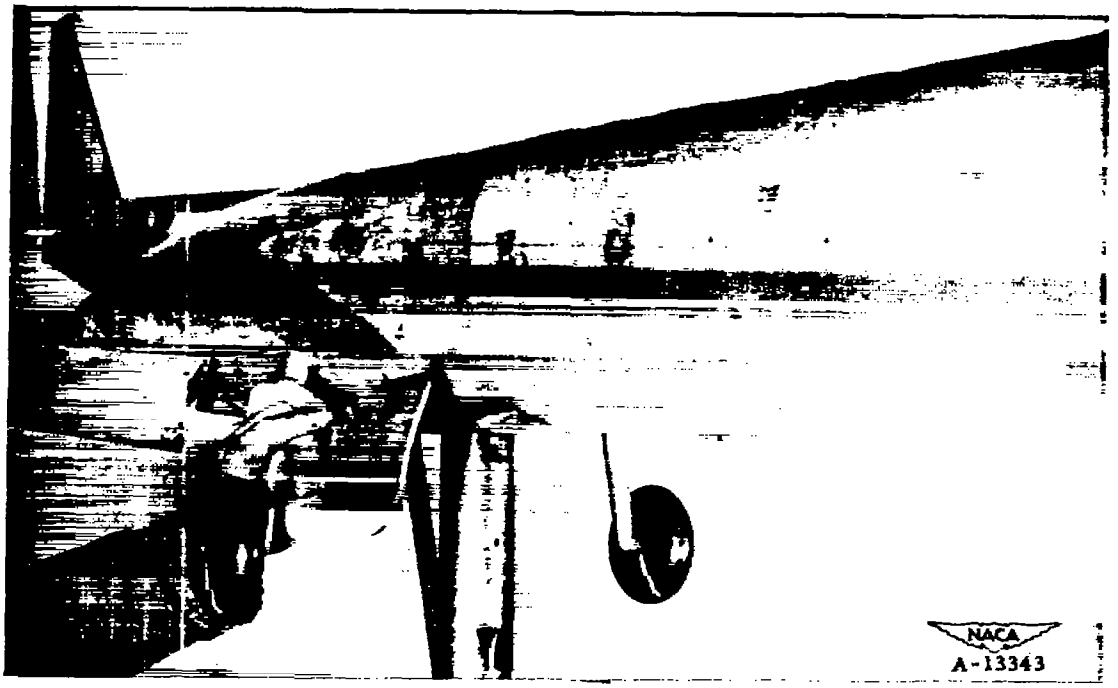

(a) Main landing gear and doors.

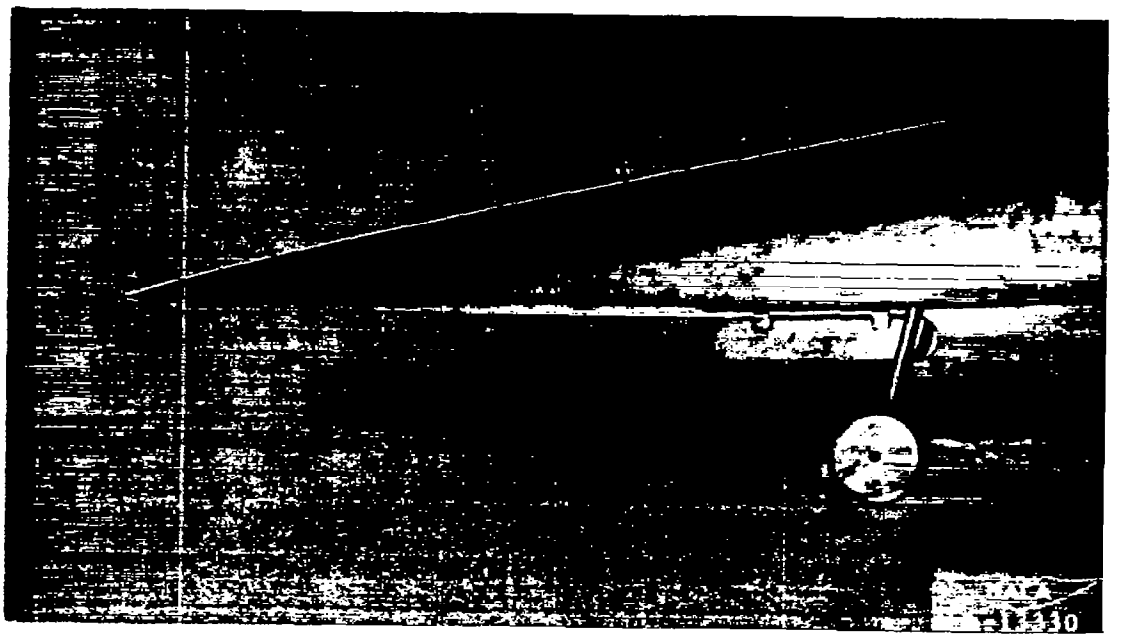

(b) Nose landing gear and door.

Figure 6.— Details of the landing gear and the landing-gear doors.

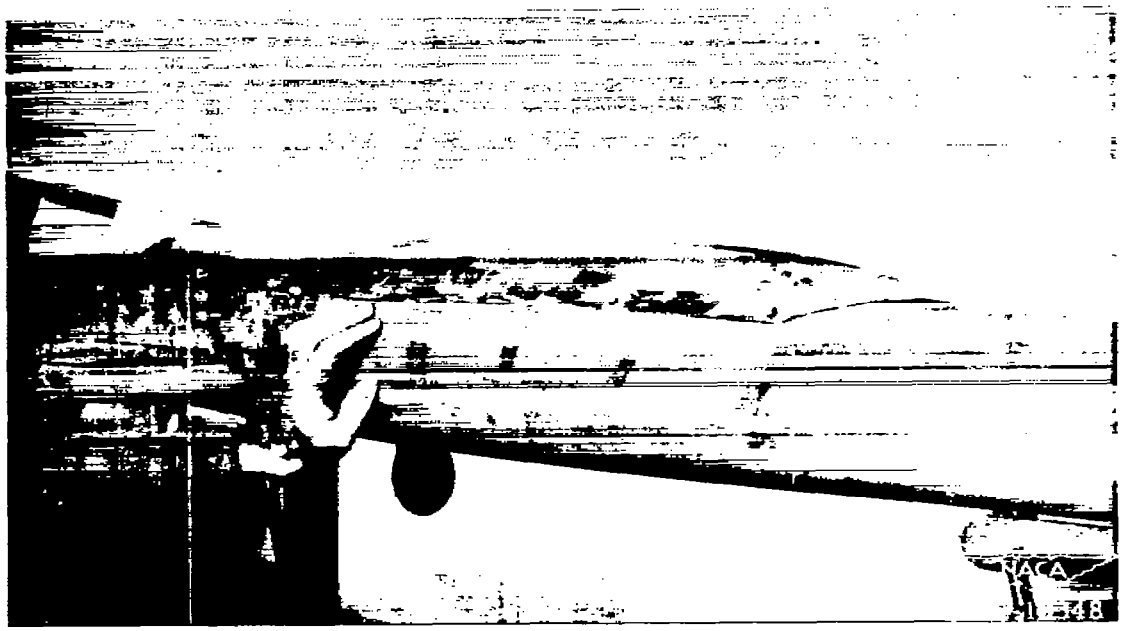

(a) Canopy

(b) Air scoops.

Figure 7.— Details of the canopy, the air scoops, and the jettisonable-nose fins.

(c) Jettisonable-nose fins.

Figure 7.- Concluded.

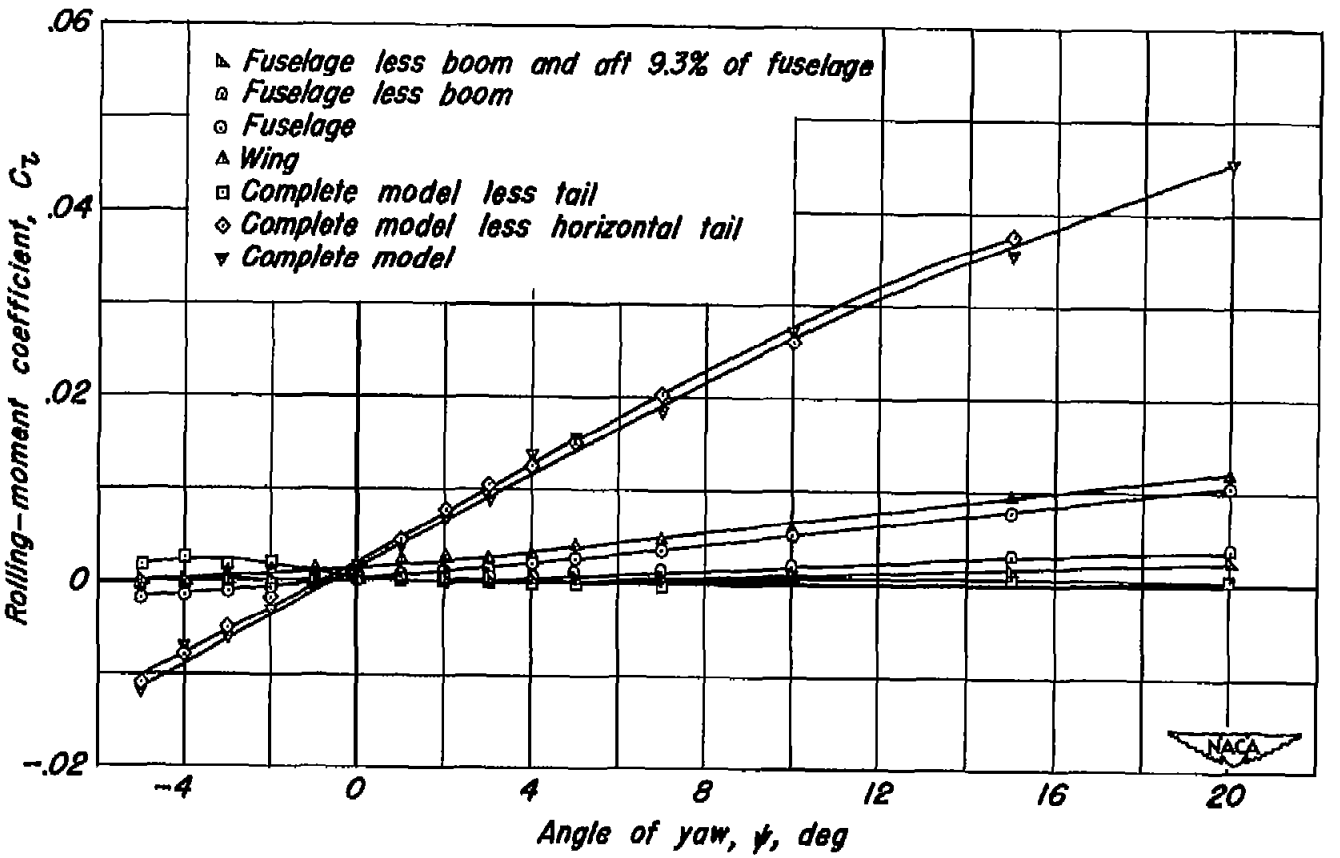

(a) Flaps neutral, $\alpha = 0°$.

Figure 8.—Effect of the component parts of the model on the variation of rolling-moment coefficient with angle of yaw.

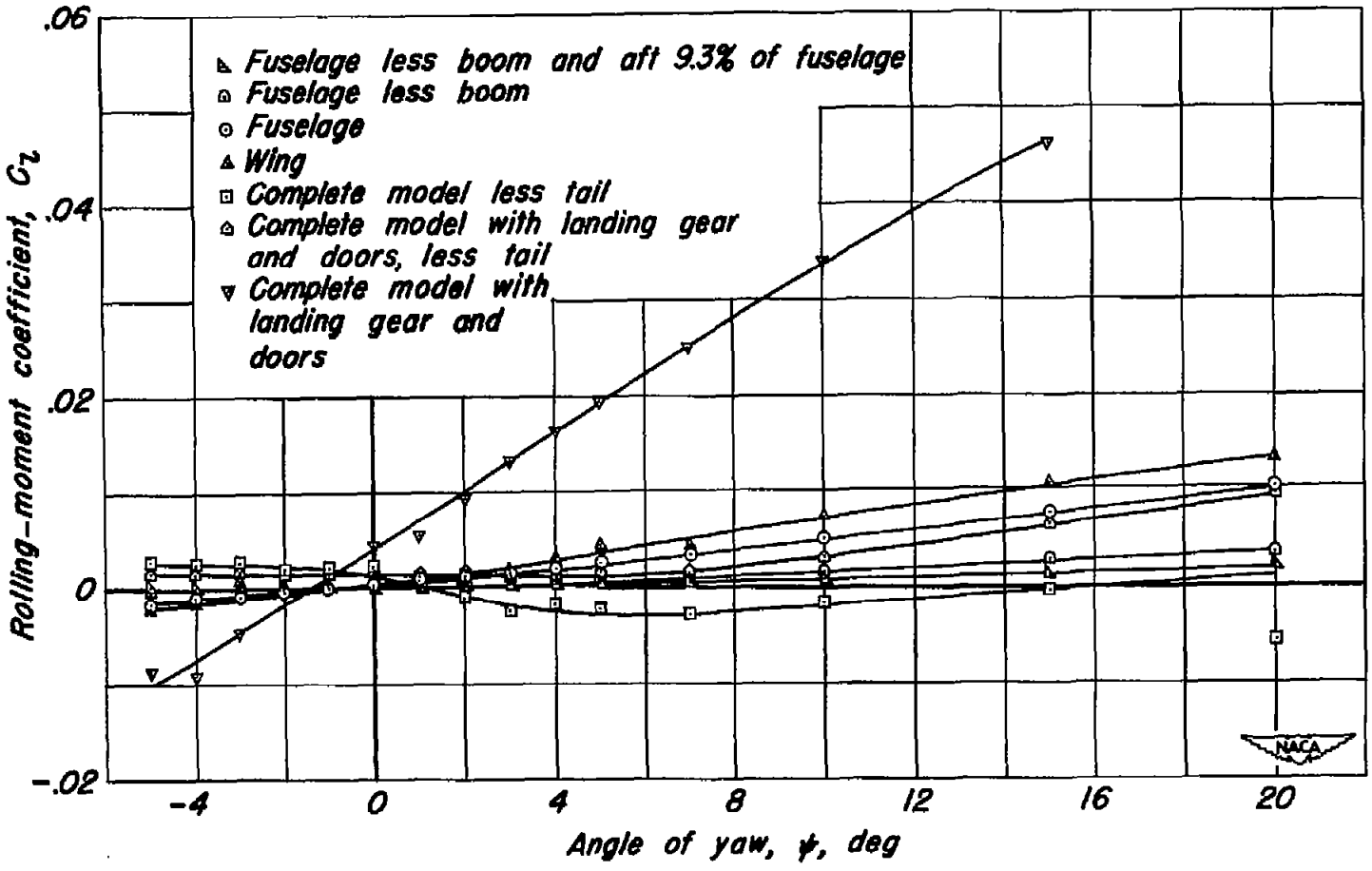

(b) $\delta_{LF} = 30°$, $\delta_{TF} = 50°$, $\alpha = 0°$.

Figure 8.—Concluded.

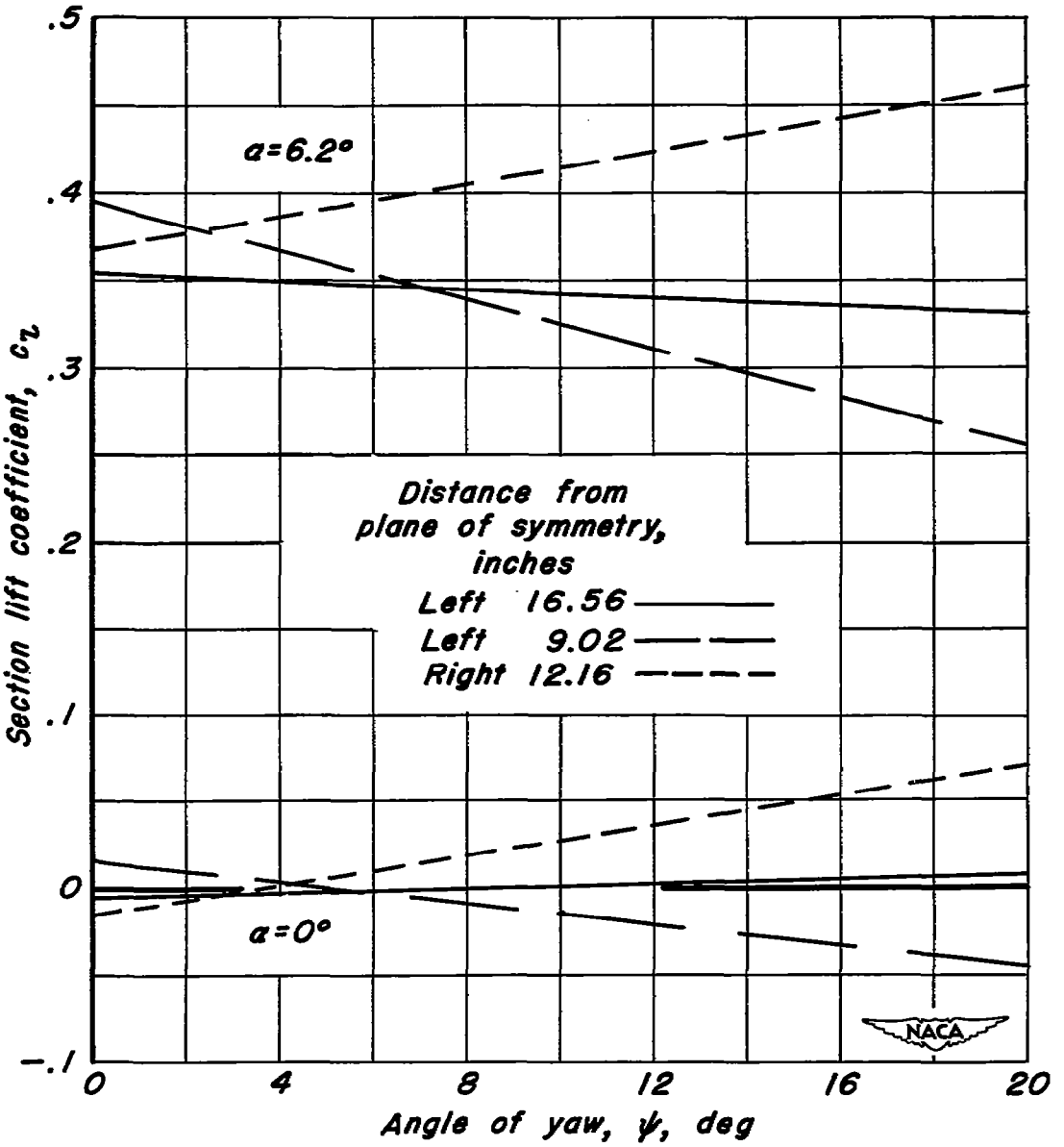

Figure 9.—Variation of wing section-lift coefficient with angle of yaw for the complete model less tail. Flaps neutral.

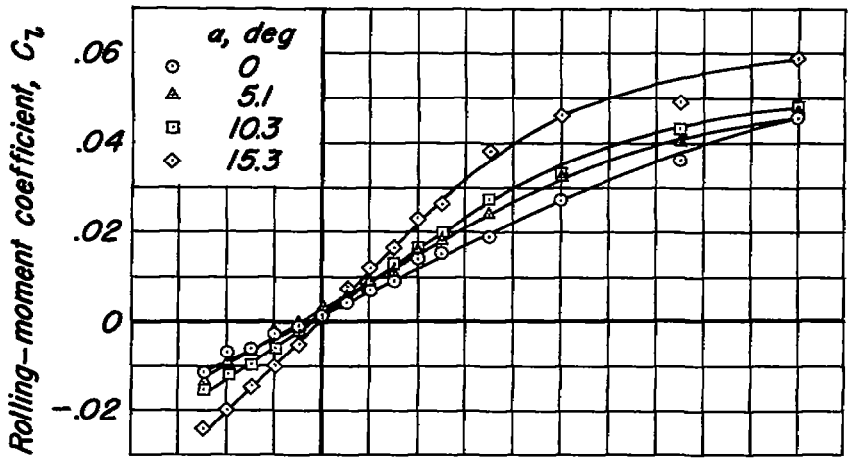

(a) Flaps neutral.

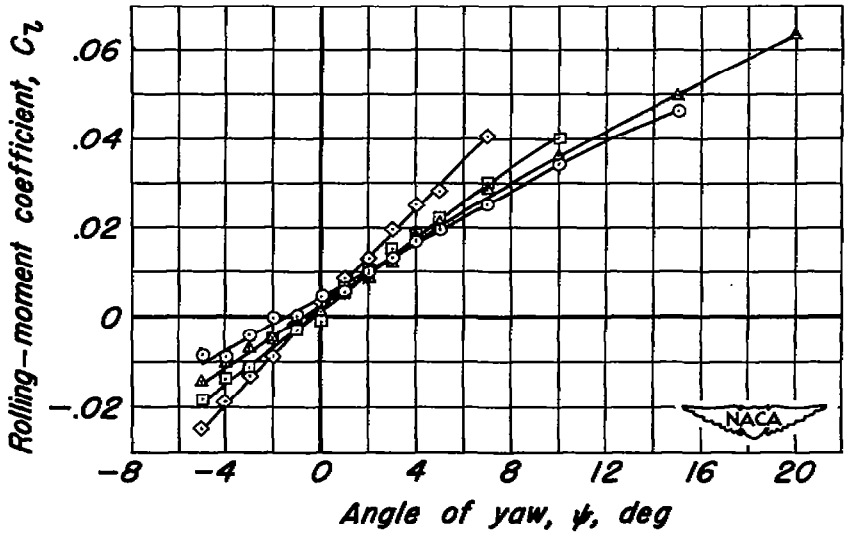

(b) $\delta_{LF}=30°$, $\delta_{TF}=50°$, landing gear and doors down.

Figure 10.— Effect of angle of attack on the variation of rolling-moment coefficient with angle of yaw for the complete model.

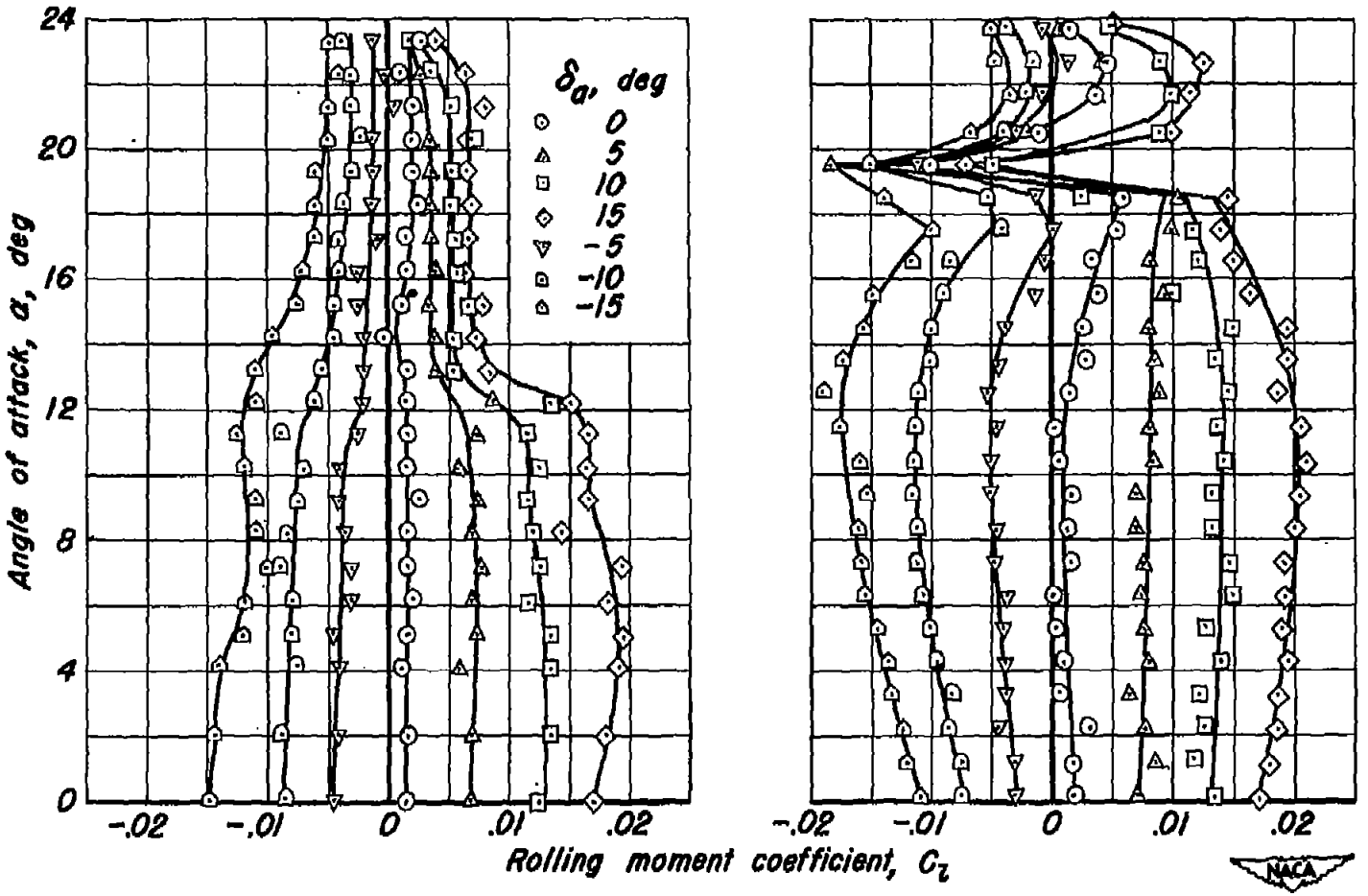

(a) Flaps neutral.

(b) $\delta_{LF}=30°$, $\delta_{TF}=50°$.

Figure 11.—Variation of aileron effectiveness with angle of attack for the complete model less tail.

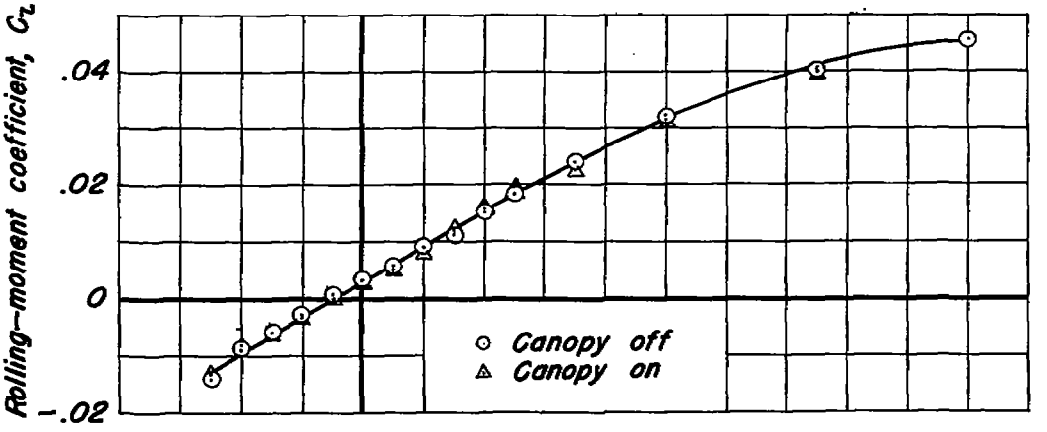

(a) Flaps neutral, $\alpha = 5.1°$.

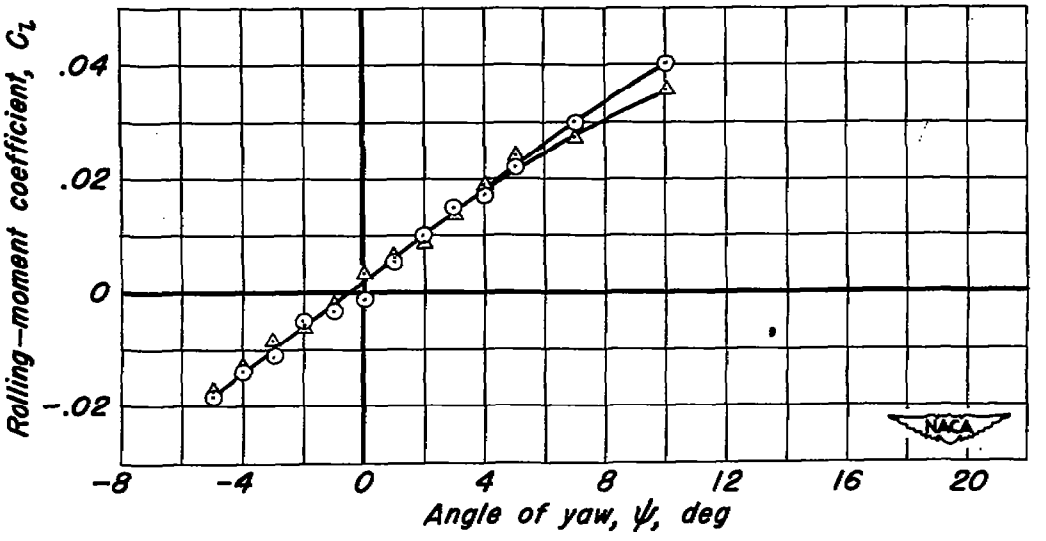

(b) $\delta_{LF} = 30°$, $\delta_{TF} = 50°$, landing gear and doors down, $\alpha = 10.3°$.

Figure 12.—Effect of the canopy on the variation of rolling-moment coefficient with angle of yaw for the complete model.

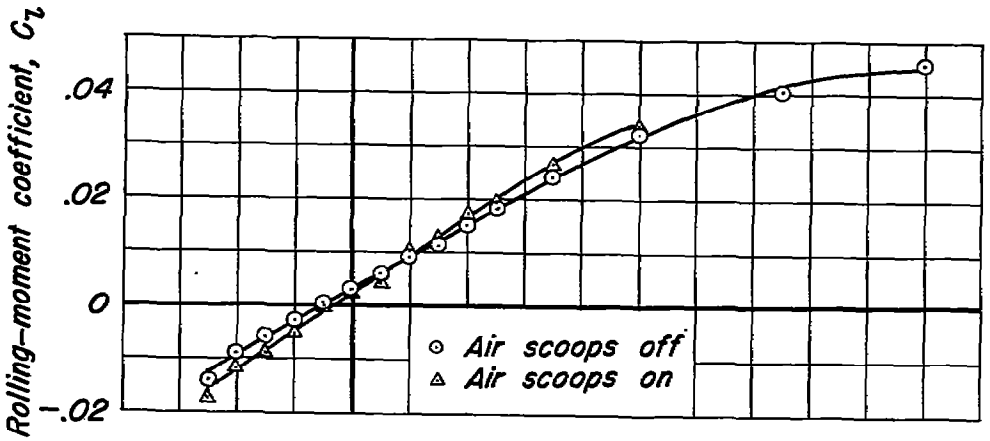

(a) Flaps neutral, $\alpha = 5.1°$.

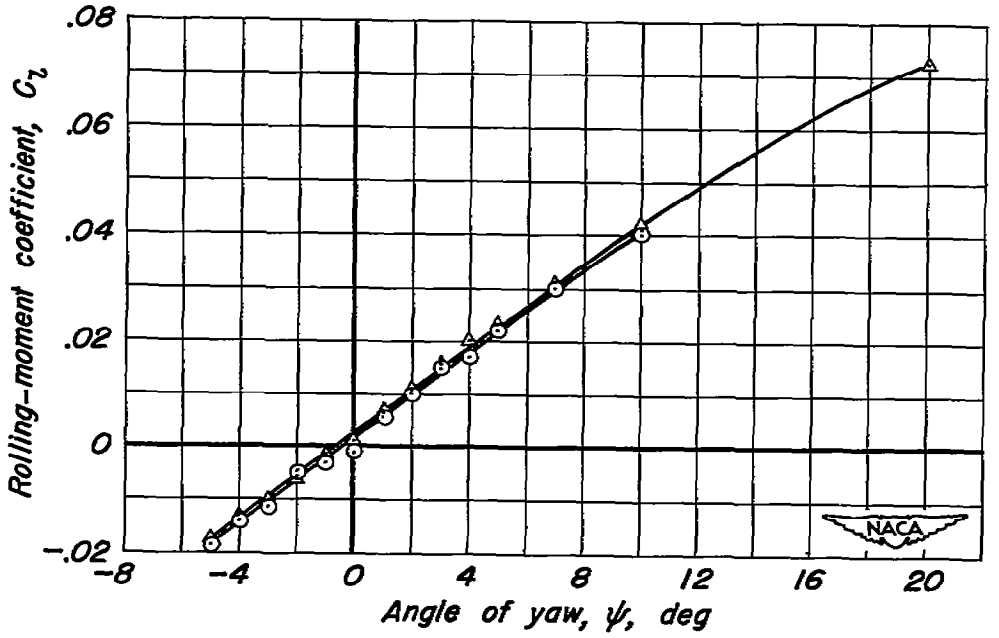

(b) $\delta_{LF} = 30°$, $\delta_{TF} = 50°$, landing gear and doors down, $\alpha = 10.3°$.

Figure 13.—Effect of the air scoops on the variation of rolling-moment coefficient with angle of yaw for the complete model.

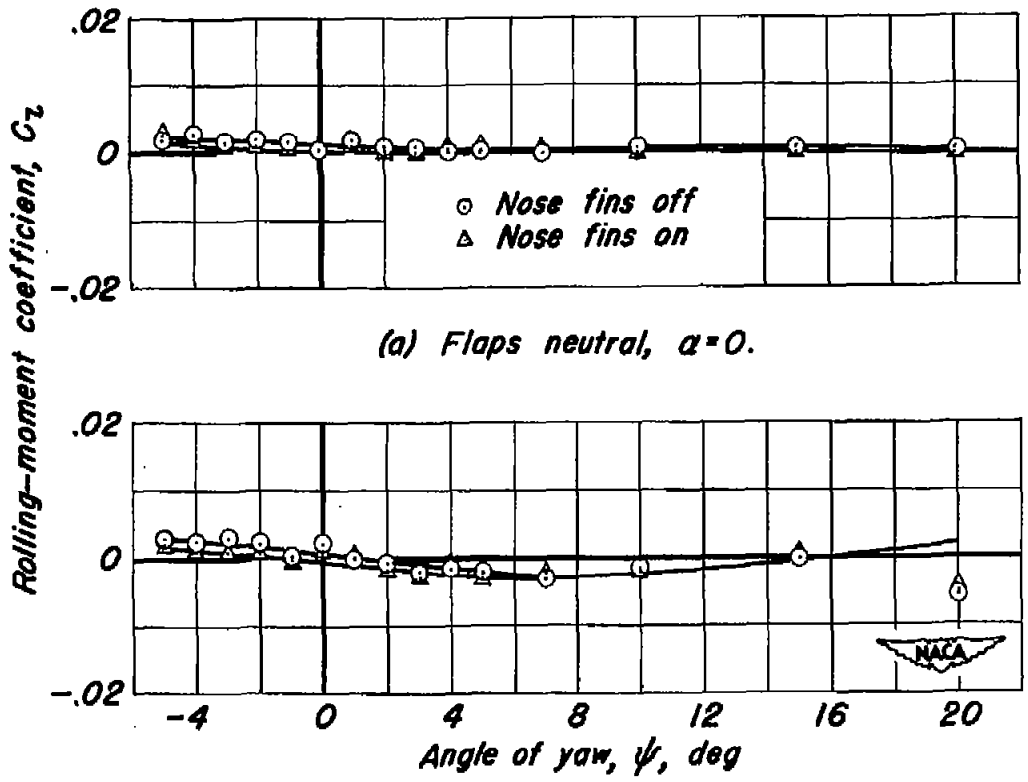

Figure 14.—Effect of nose fins on the variation of rolling-moment coefficient with angle of yaw for the complete model less tail.

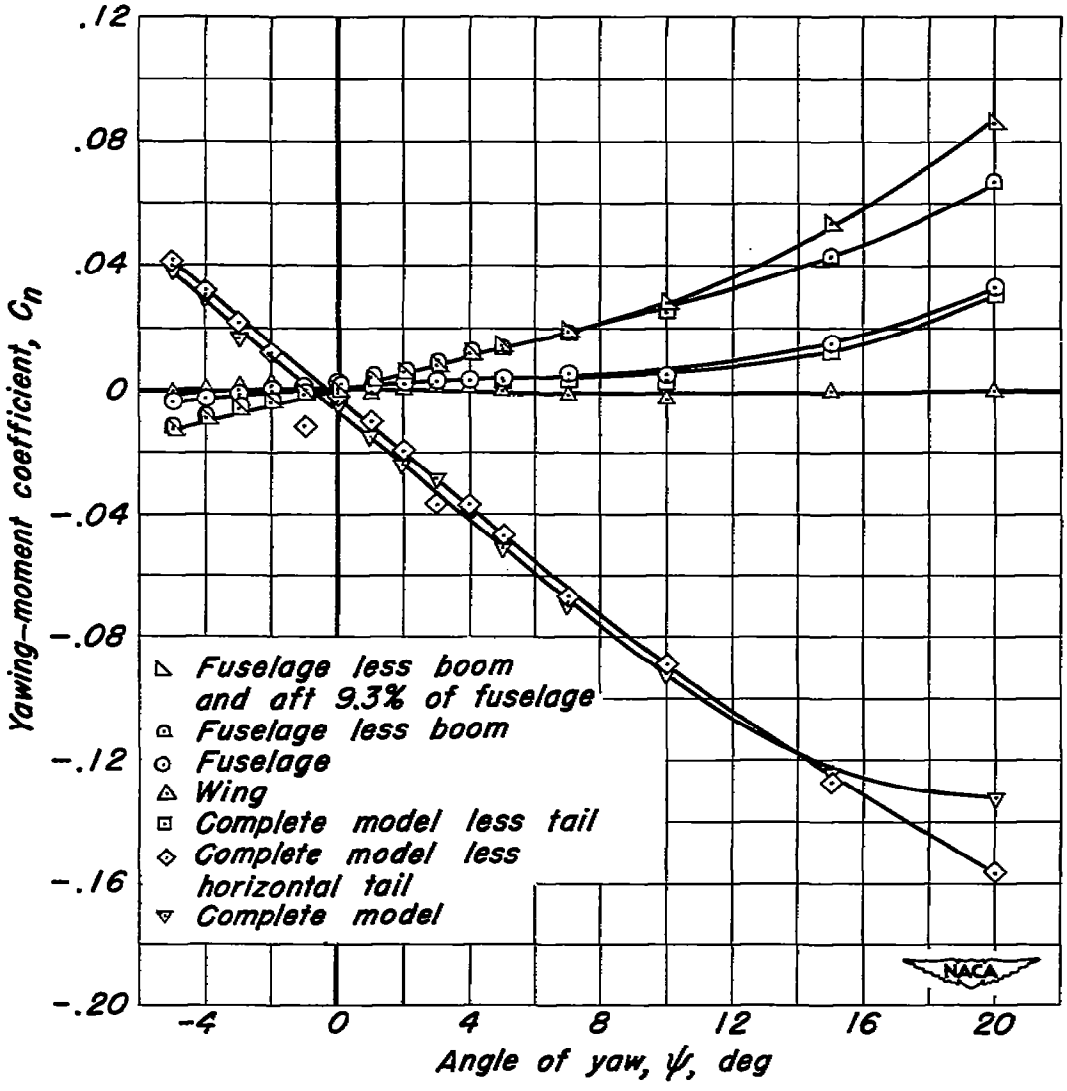

(a) Flaps neutral, $\alpha = 0$.

Figure 15.—Effect of the component parts of the model on the variation of yawing-moment coefficient with the angle of yaw.

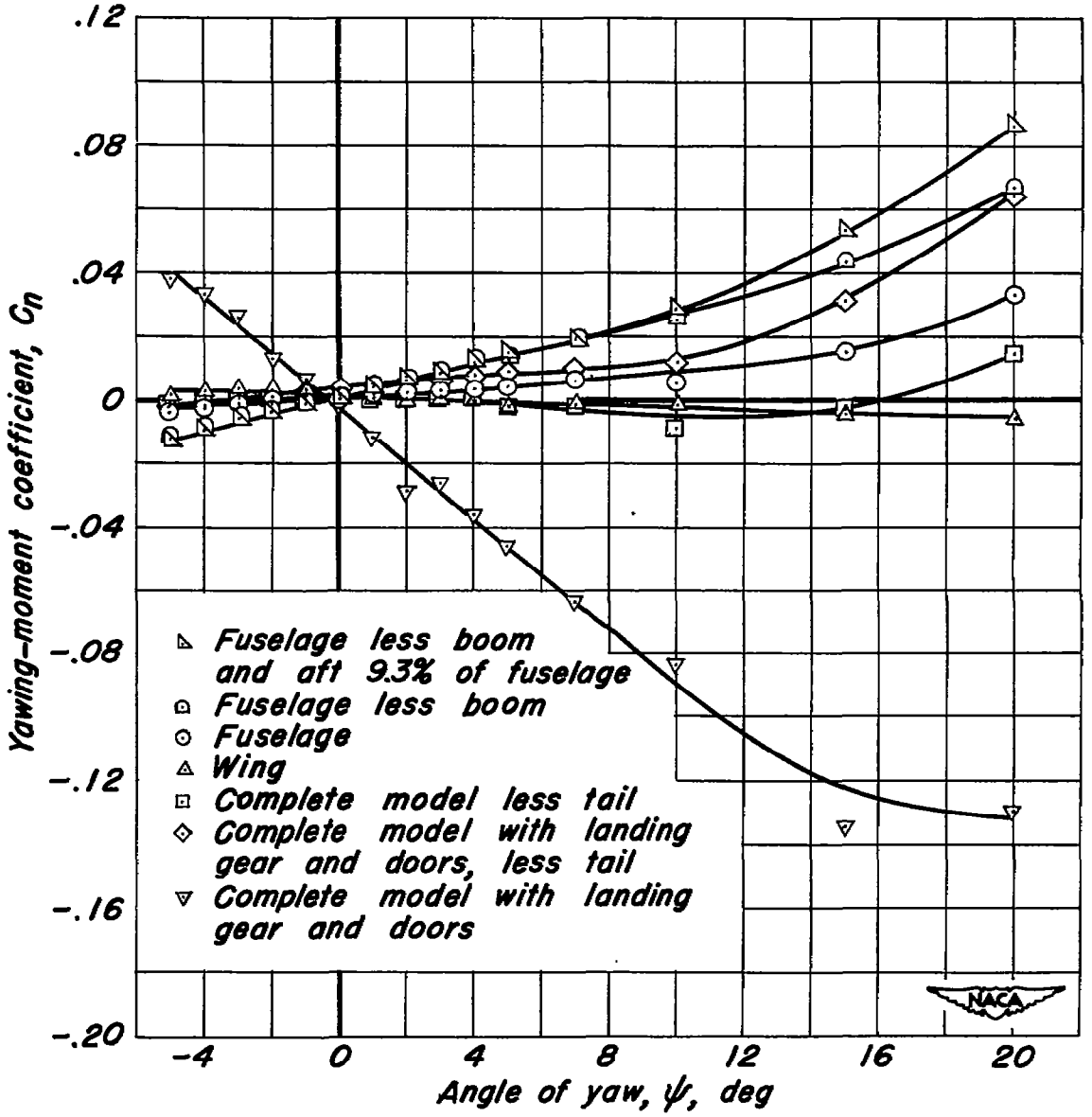

(b) $\delta_{LF} = 30°$, $\delta_{TF} = 50°$, $\alpha = 0$.

Figure 15.— Concluded.

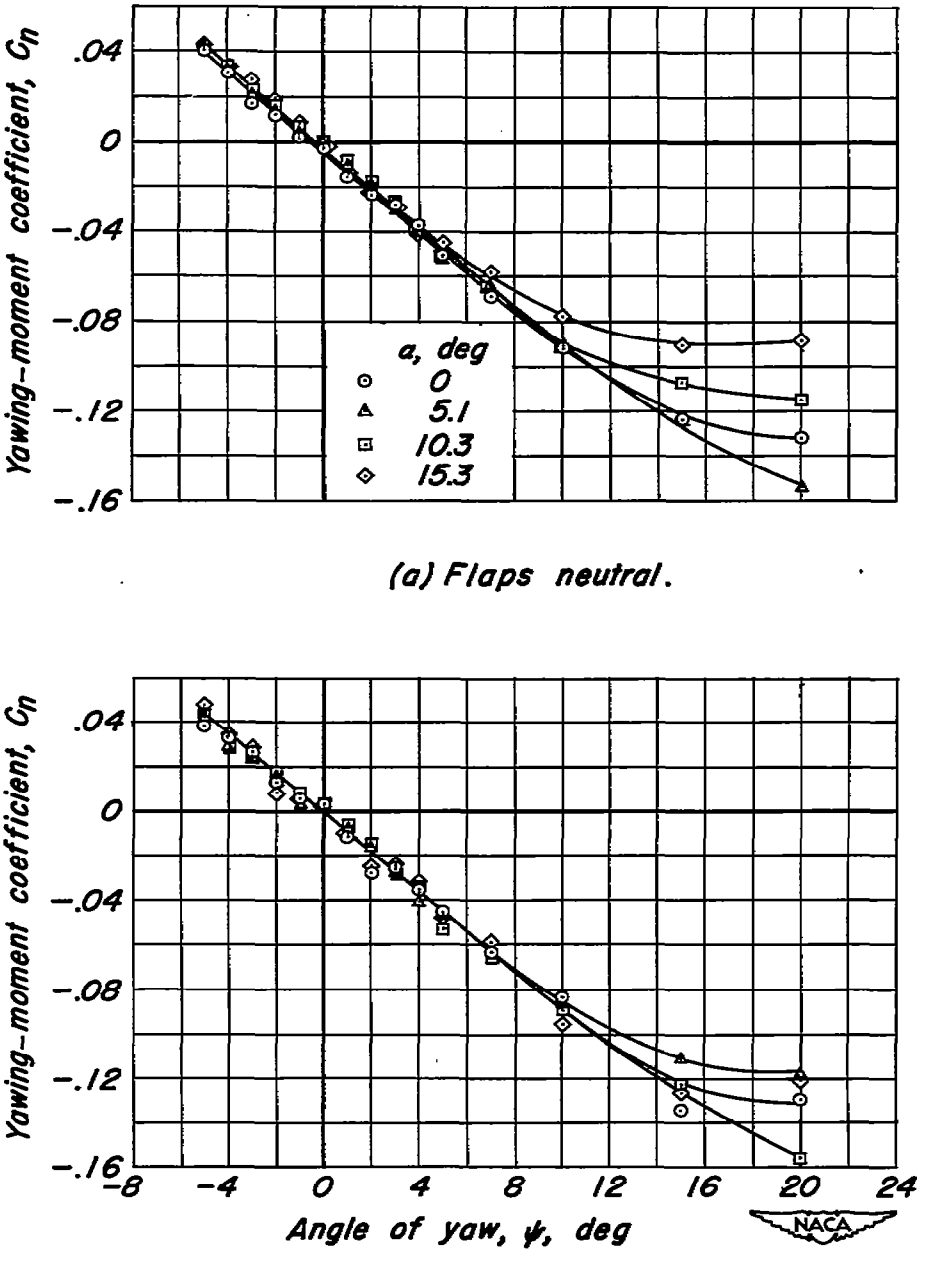

(a) Flaps neutral.

(b) $\delta_{LF} = 30°$, $\delta_{TF} = 50°$, landing gear and doors down.

Figure 16.—Effect of angle of attack on the variation of yawing-moment coefficient with angle of yaw for the complete model.

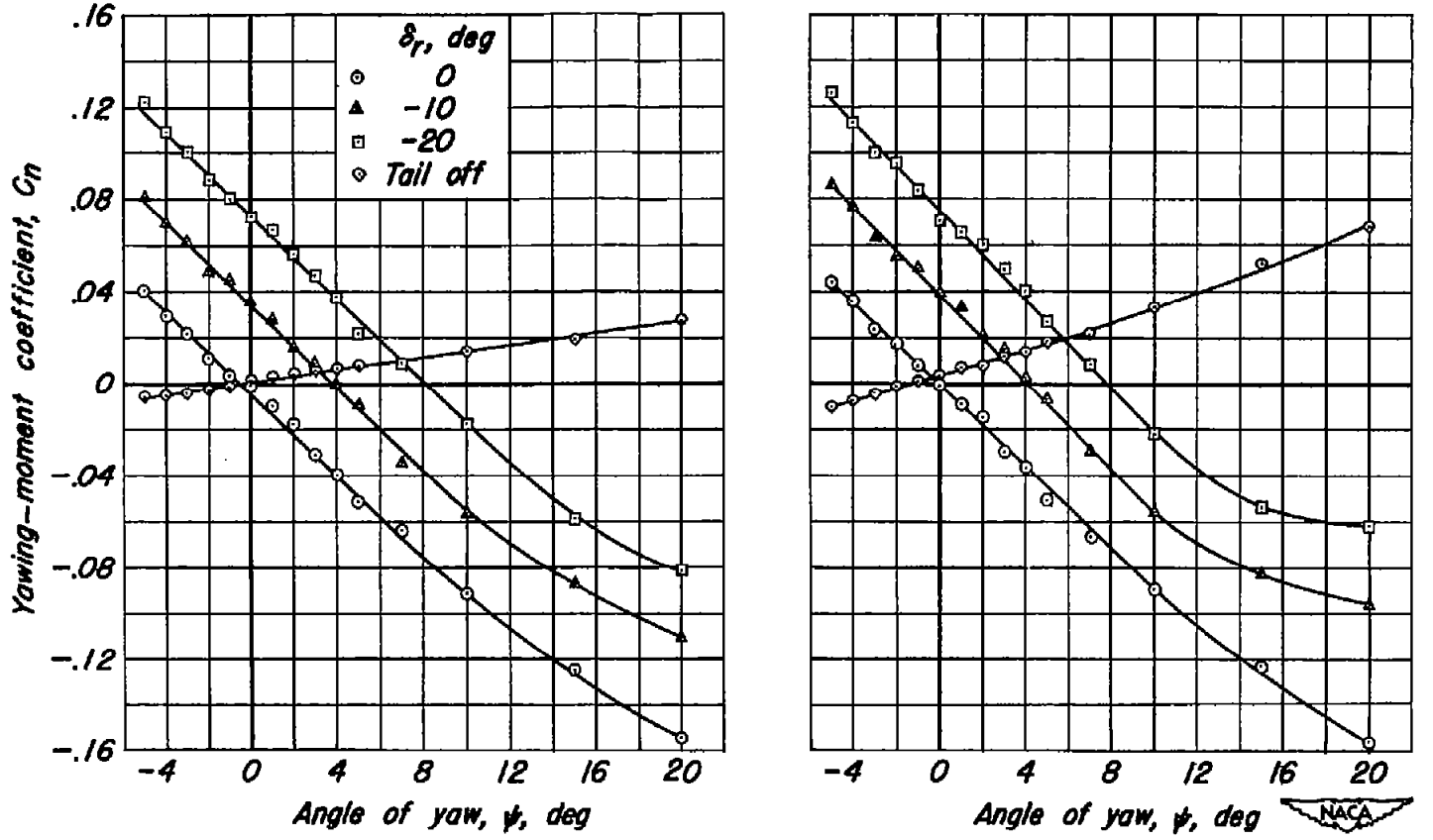

(a) Flaps neutral, $\alpha = 5.1°$.

(b) $\delta_{LF} = 30°$, $\delta_{TF} = 50°$, landing gear and doors down, $\alpha = 10.3°$.

Figure 17.— Effect of rudder deflection on the variation of yawing-moment coefficient with angle of yaw for the complete model.

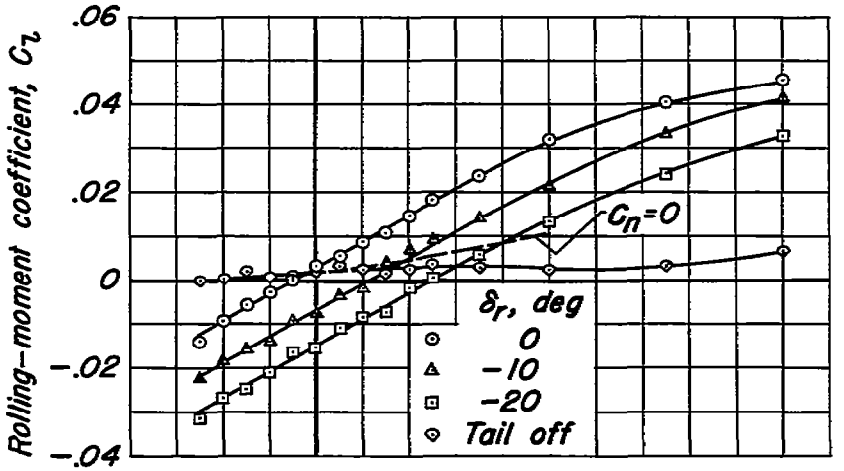

(a) Flaps neutral, α= 5.1°

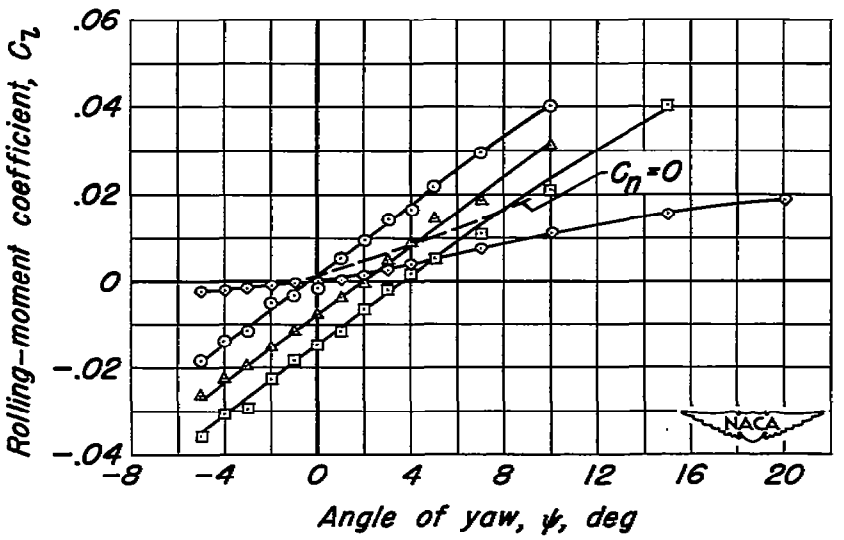

(b) δ_{LF}= 30°, δ_{TF}=50°, landing gear and doors down, α=10.3°.

Figure 18.— Effect of rudder deflection on the variation of rolling-moment coefficient with angle of yaw for the complete model.

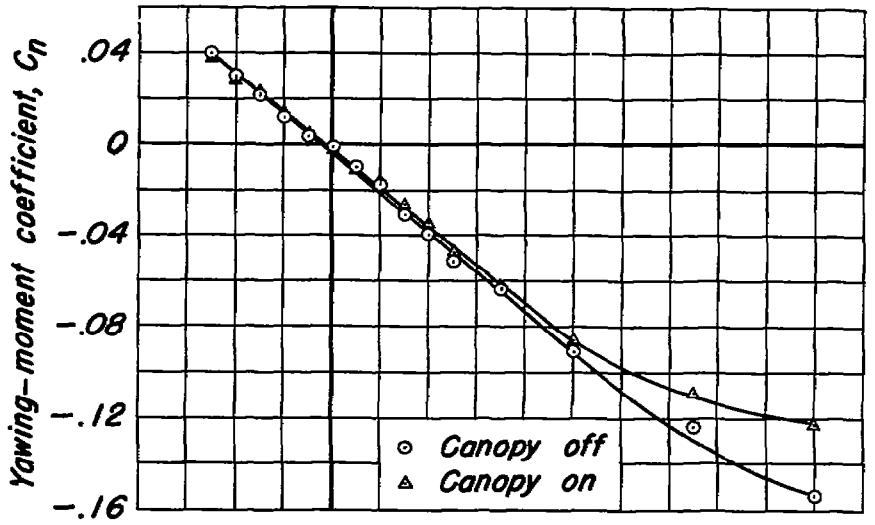

(a) Flaps neutral, $\alpha = 5.1°$.

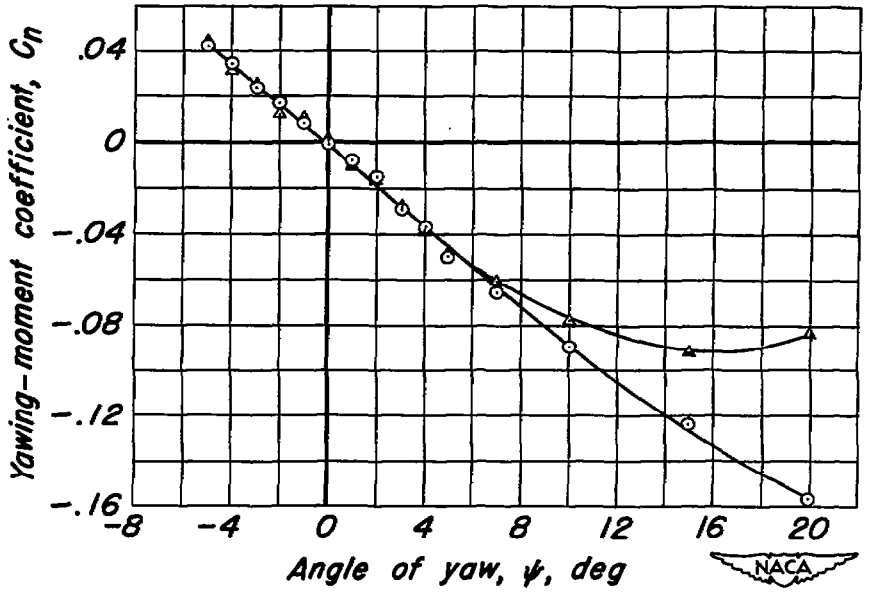

(b) $\delta_{LF} = 30°$, $\delta_{TF} = 50°$, landing gear and doors down, $\alpha = 10.3°$.

Figure 19.—Effect of the canopy on the variation of yawing-moment coefficient with angle of yaw for the complete model.

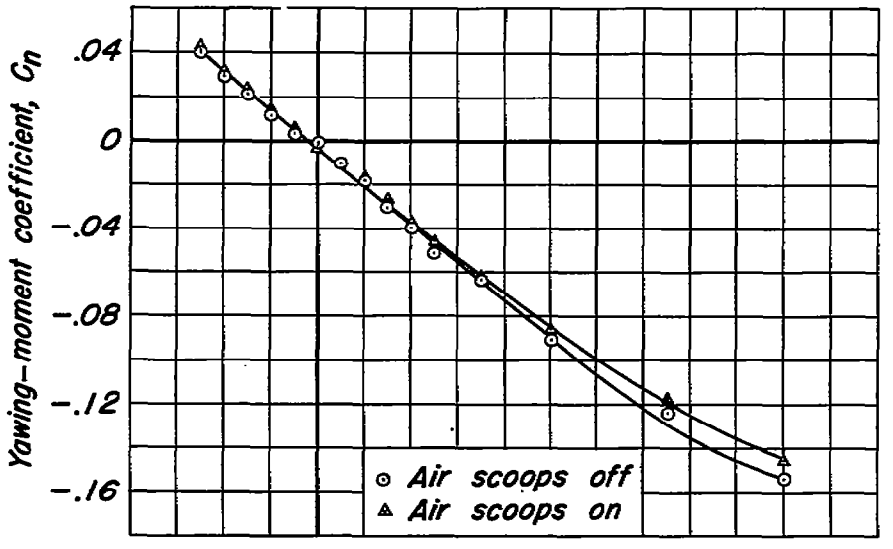

(a) Flaps neutral, $\alpha = 5.1°$.

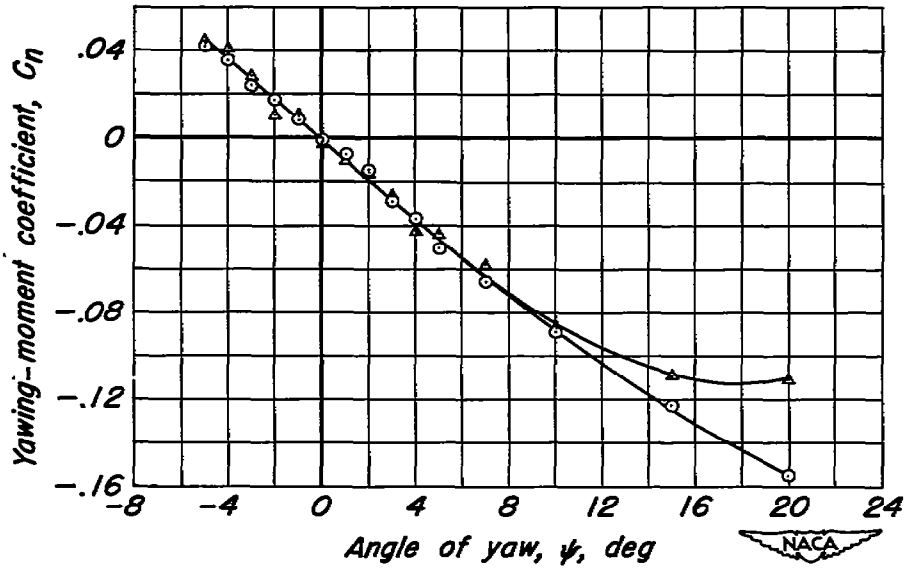

(b) $\delta_{LF} = 30°$, $\delta_{TF} = 50°$, landing gear and doors down, $\alpha = 10.3°$.

Figure 20.—Effect of the air scoops on the variation of yawing-moment coefficient with angle of yaw for the complete model.

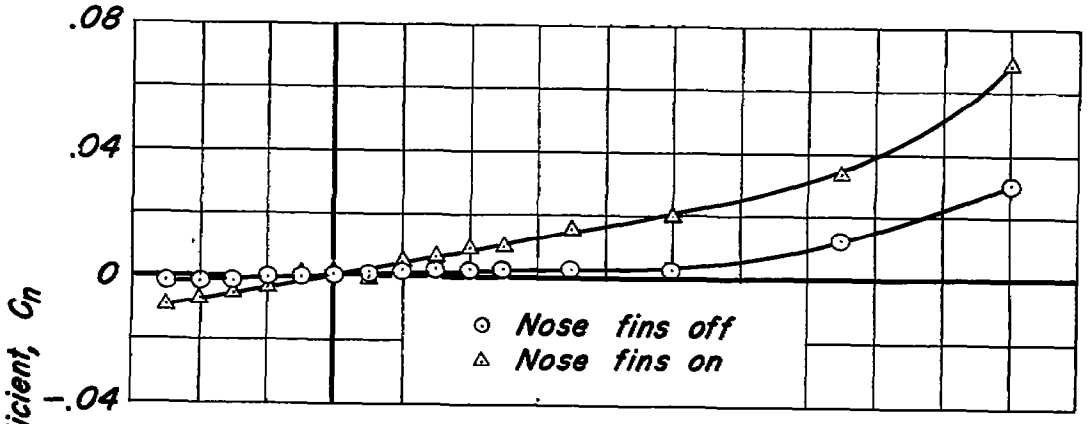

(a) Flaps neutral, $\alpha=0$.

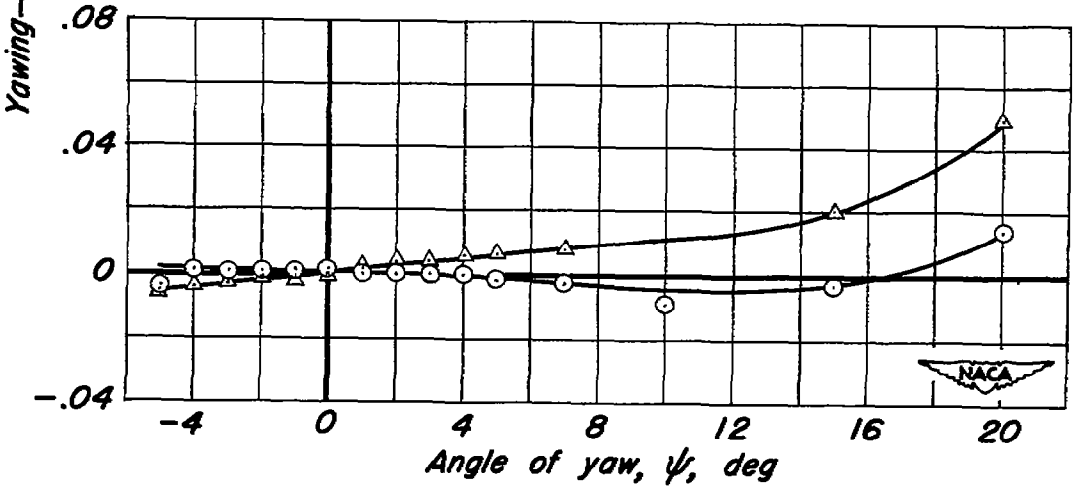

(b) $\delta_{LF}=30°$, $\delta_{TF}=50°$, $\alpha=0$.

Figure 21.—Effect of nose fins on the variation of yawing-moment coefficient with angle of yaw for the complete model less tail.

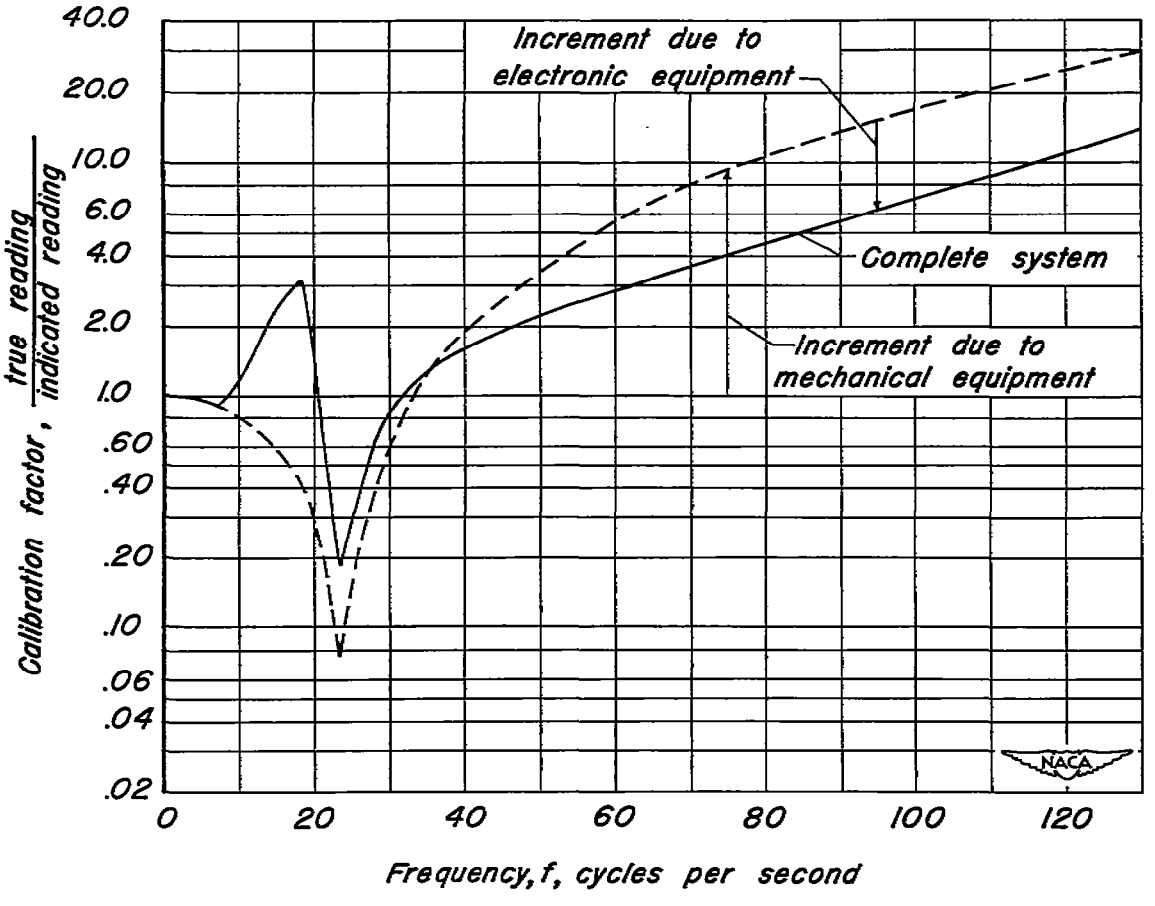

Figure 22.—Variation of calibration factor with frequency for the equipment used in measuring the variation of rolling moment with time.

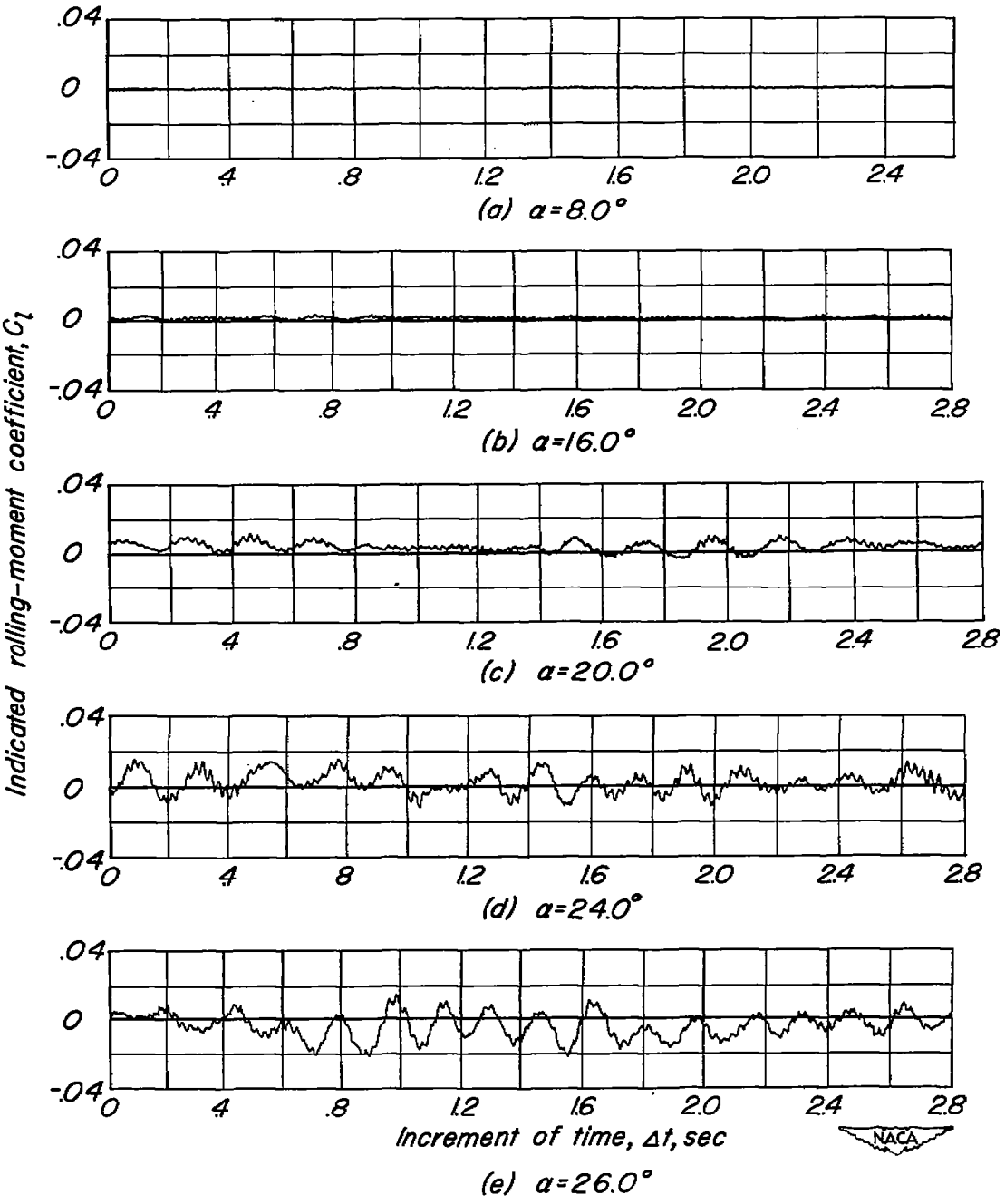

Figure 23.—Variation of rolling-moment coefficient with time for the fuselage.

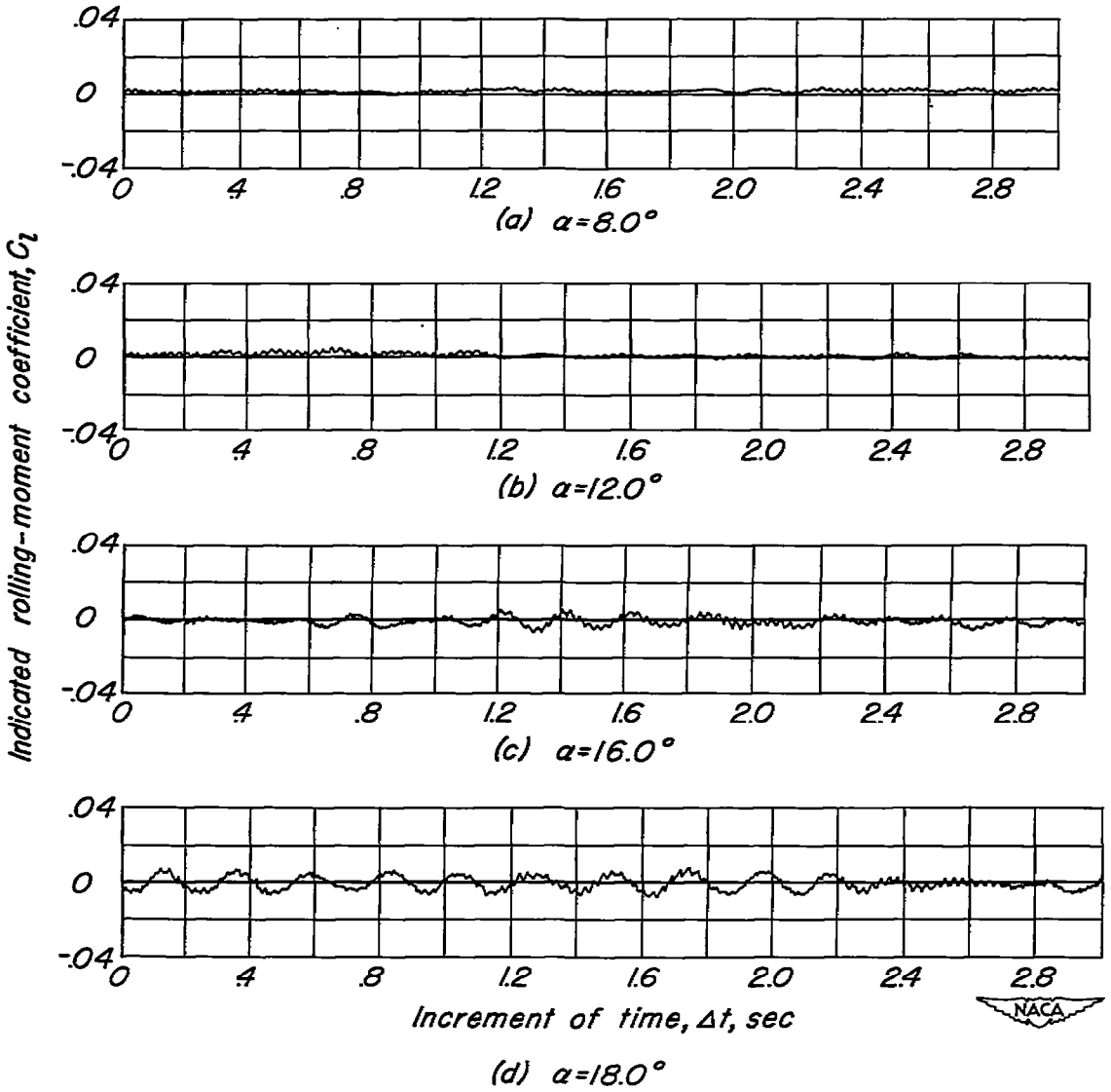

Figure 24.—Variation of rolling-moment coefficient with time for the fuselage with the tail.

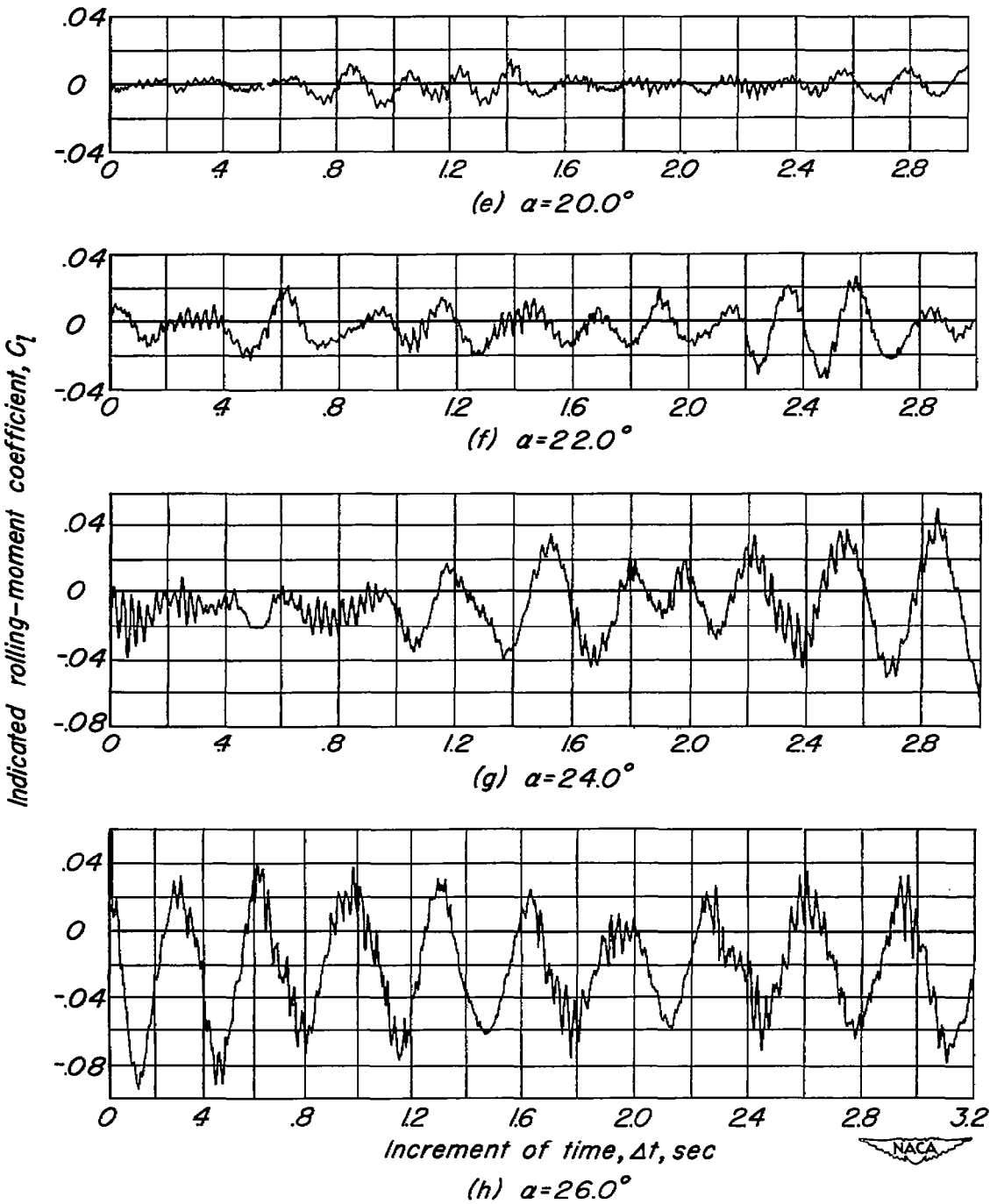

Figure 24.—Concluded

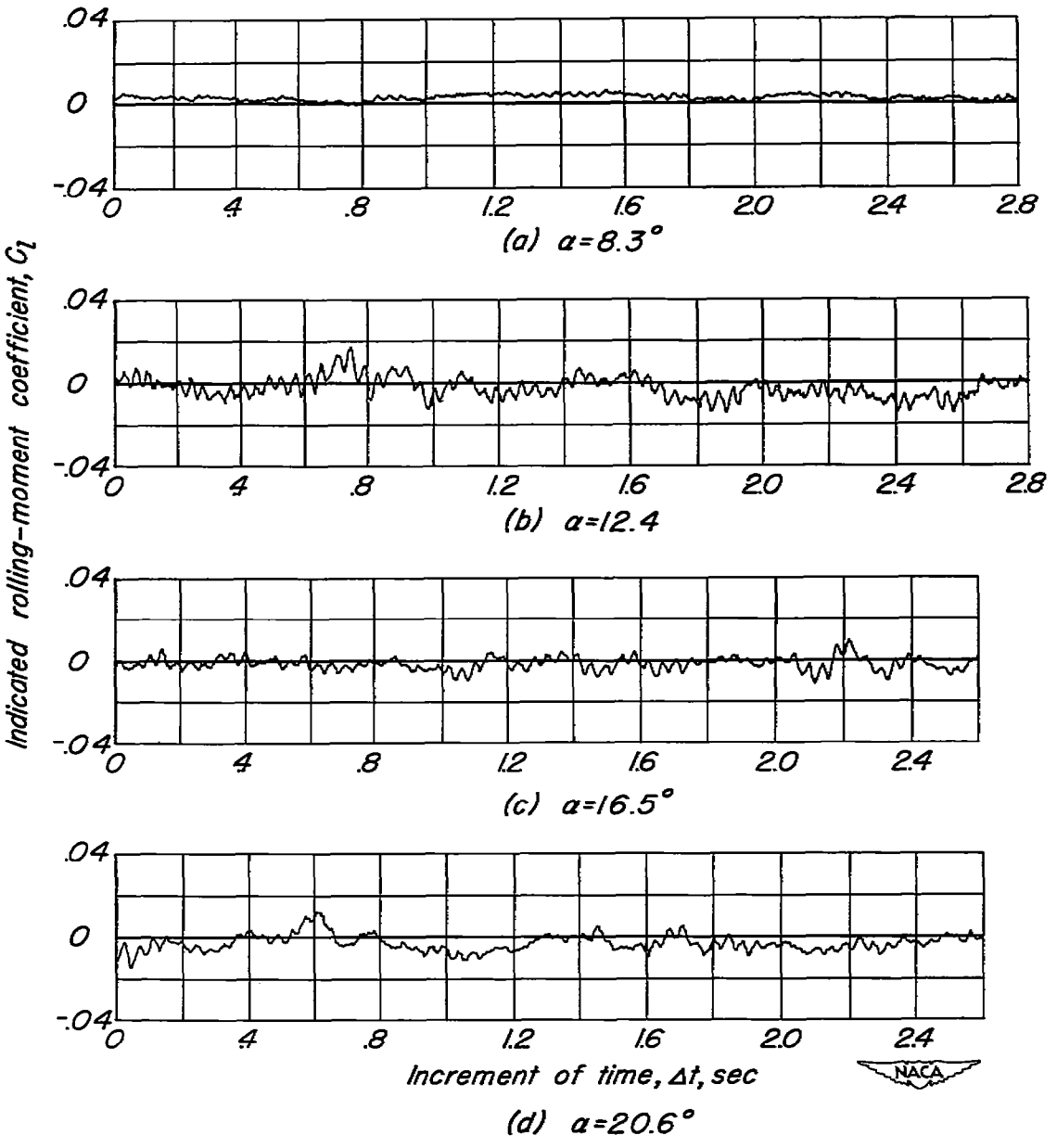

Figure 25.—Variation of rolling-moment coefficient with time for the complete model less tail. Flaps neutral.

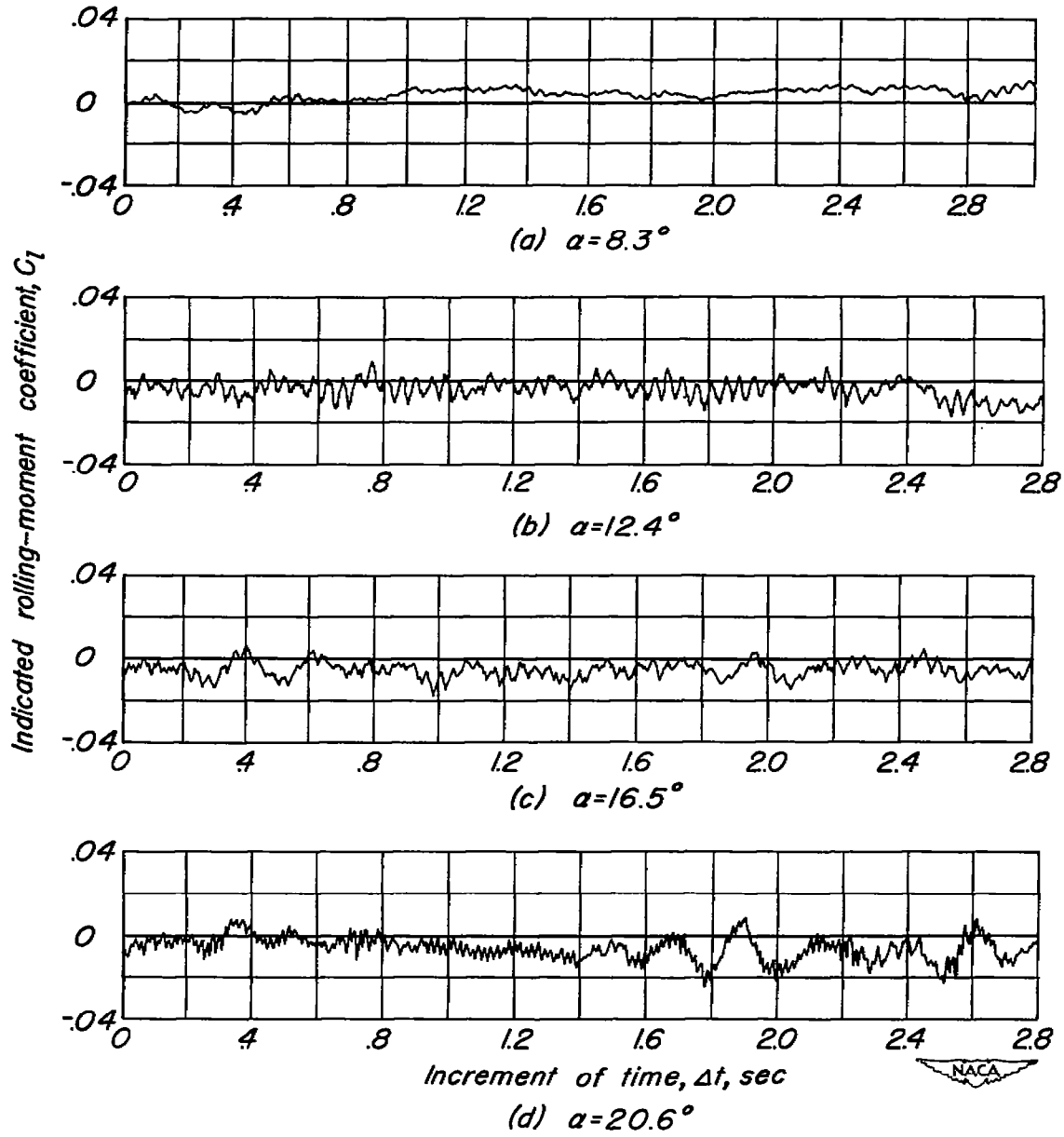

Figure 26.—Variation of rolling-moment coefficient with time for the complete model. Flaps neutral.

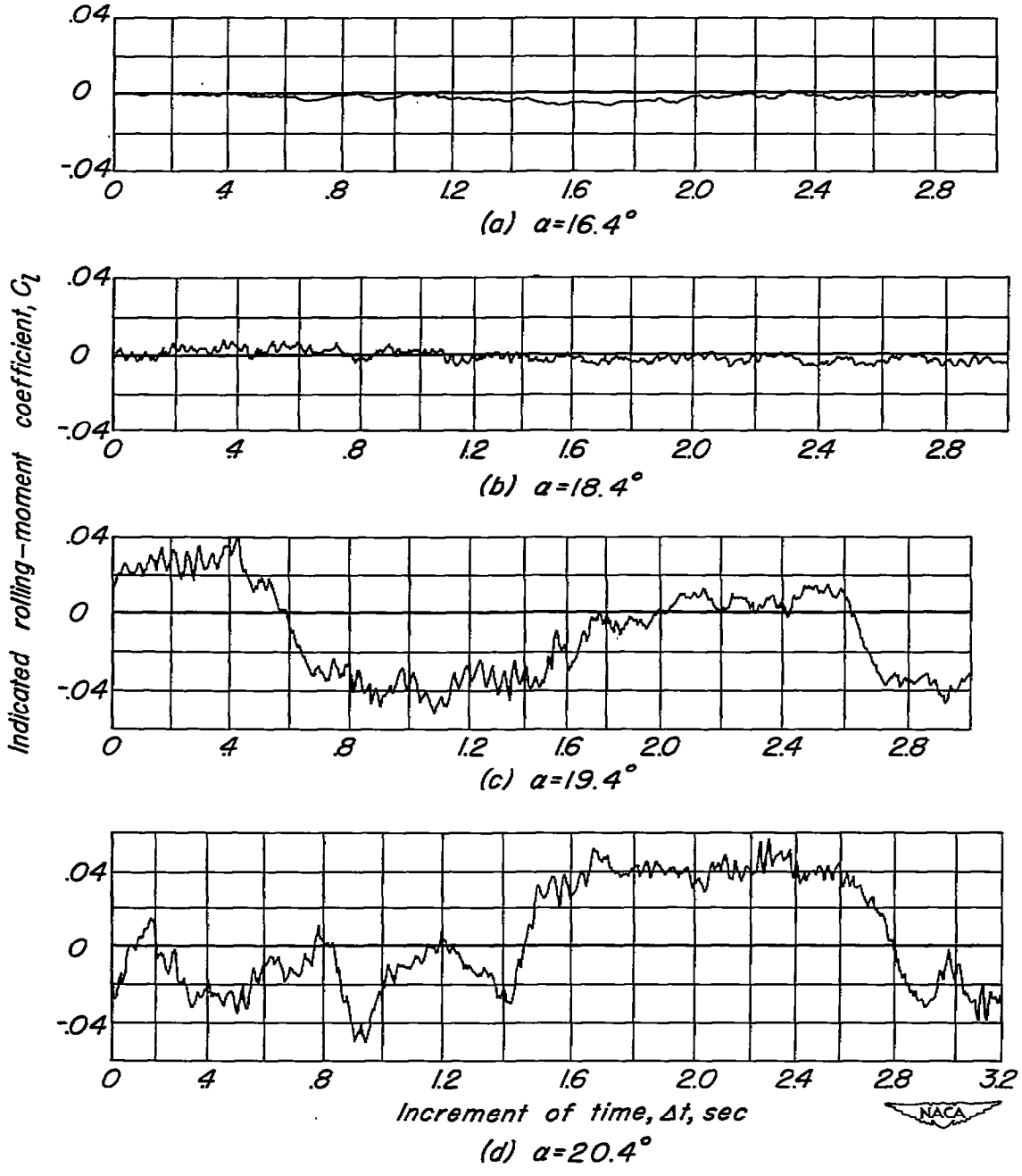

Figure 27.—Variation of rolling-moment coefficient with time for the complete model less tail. δ_{LF}=30°, δ_{TF}=50°.

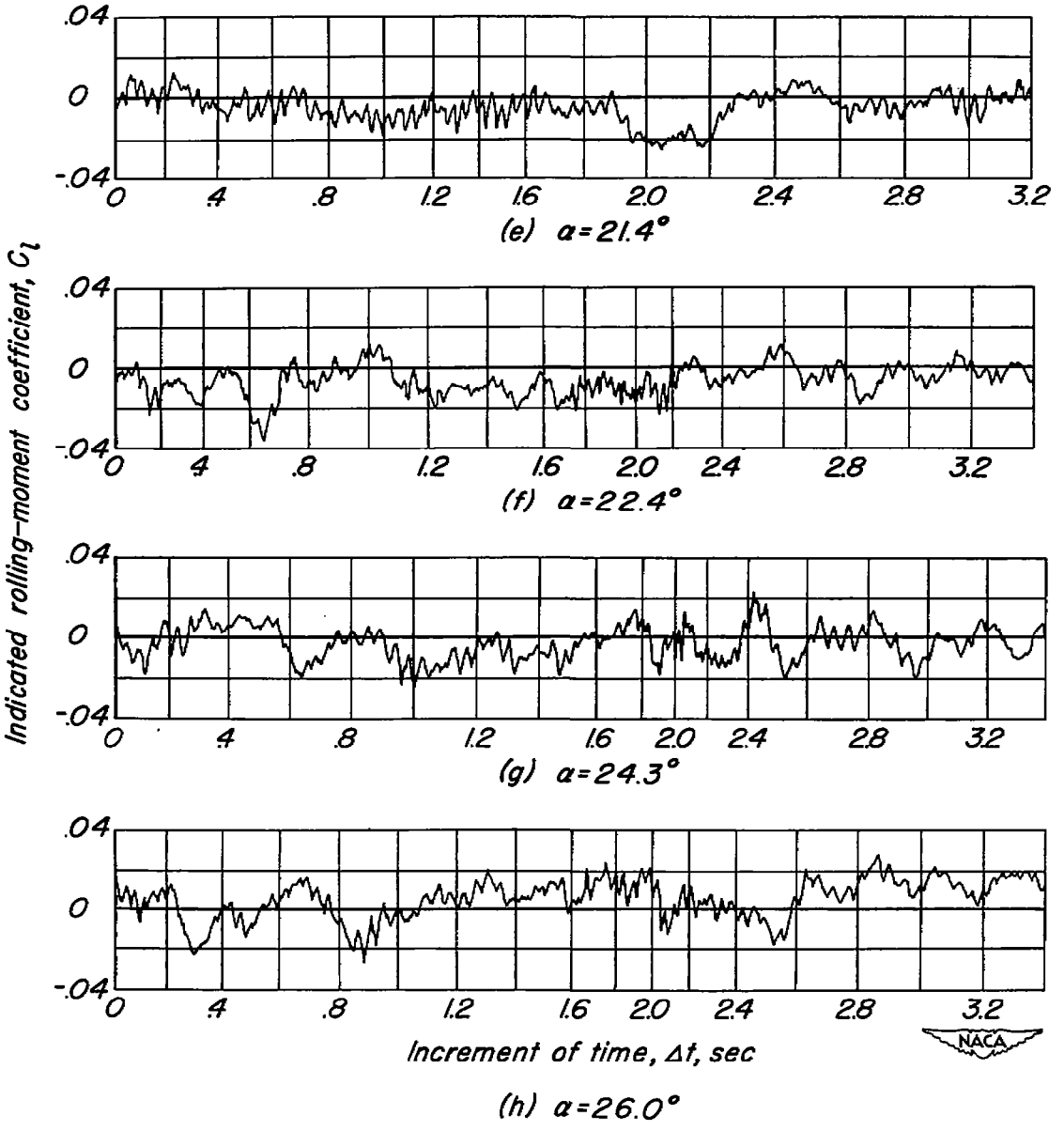

Figure 27.- Concluded.

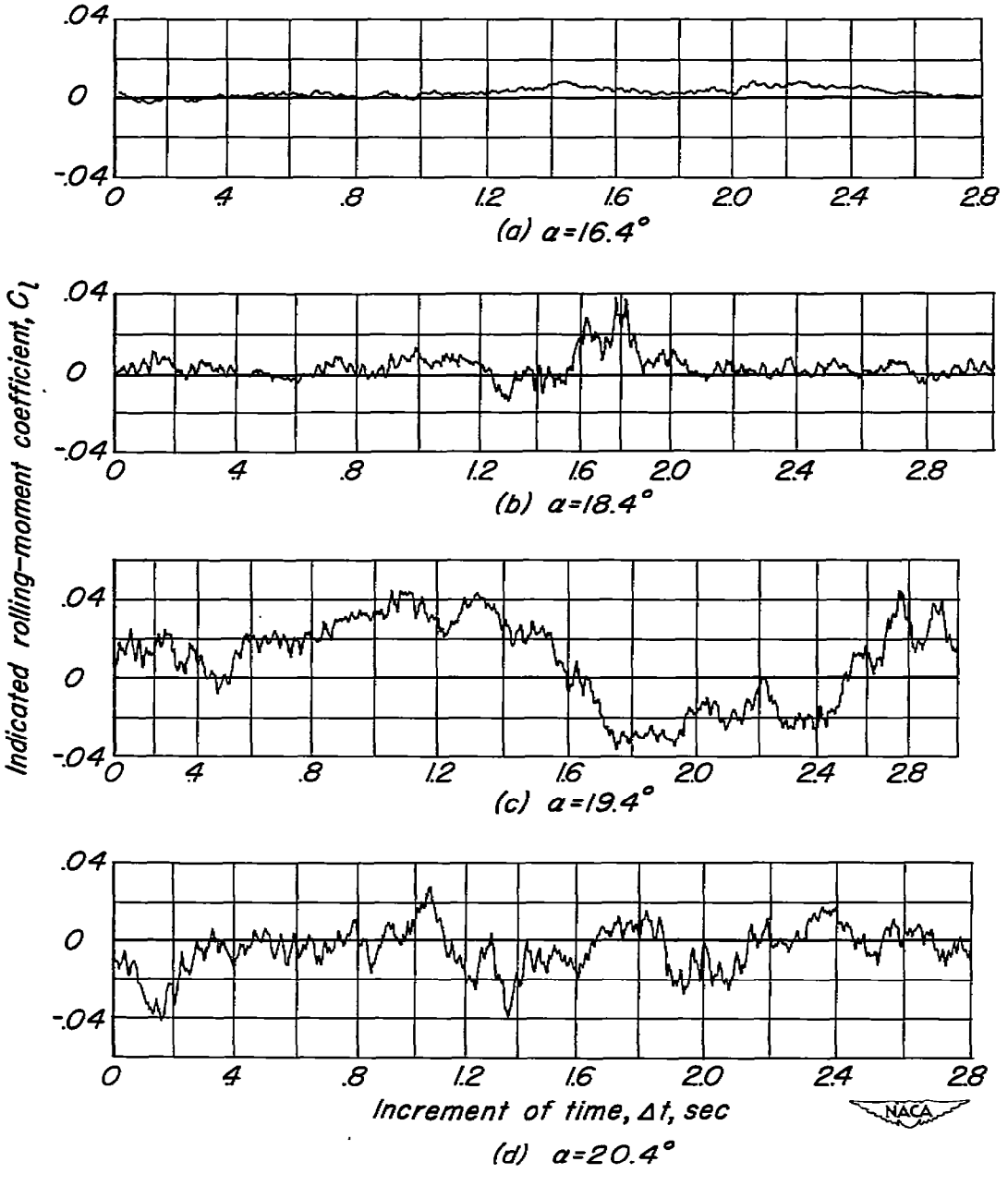

Figure 28.—Variation of rolling-moment coefficient with time for the complete model. δ_{LF}=30°, δ_{TF}=50°.

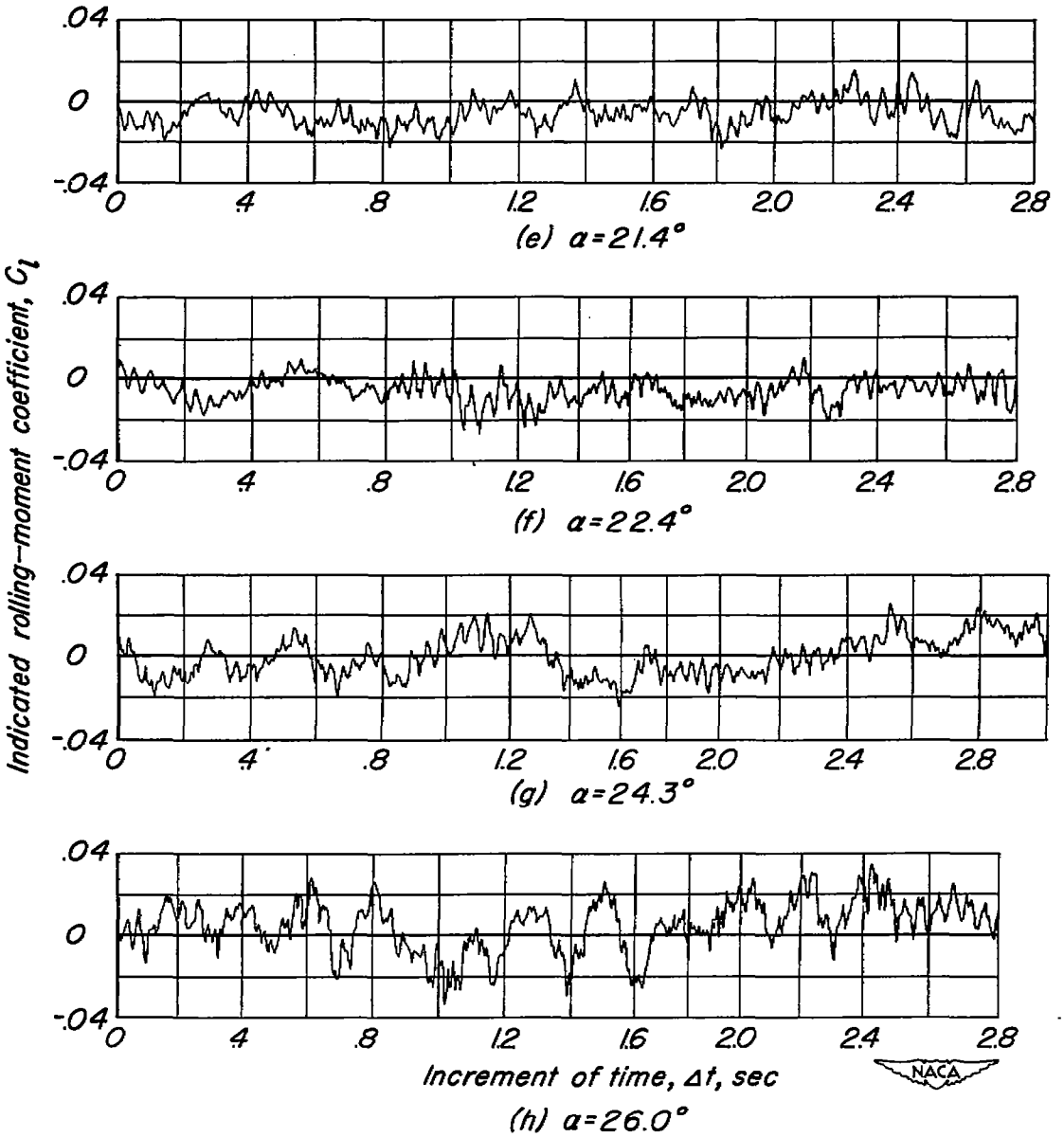

Figure 28.– Concluded.